Advances in Continuous and Discrete Models

RESEARCH Open Access

The impact of resource limitation on the pest-natural enemy ecosystem with anti-predator behavior and fear effect

Wenjie Qin[1*] and Zhengjun Dong[1]

*Correspondence:
wjqin@ymu.edu.cn;
wenjieqin@hotmail.com
[1]Department of Mathematics, Yunnan Minzu University, Kunming, 650500, P.R. China

Abstract

Research on agricultural pest control data indicates that the actual effectiveness of insecticides may exhibit slight variations, influenced by factors such as the type and quantity of pests. Additionally, the development of resistance by pests, as a result of adaptation to the environment, can impact the precision of pest control strategies. Hence we suggest implementing a nonlinear pulse state-dependent feedback control system, considering resource limitations, to investigate the influence of varying pesticide fatality rates on pest outbreaks. This paper takes into account the fear effect and anti-predator behavior to accurately portray the farmland ecosystem. We assessed the phase set and Poincaré map under the conditions for the existence of order-k (where $k = 1, 2, 3$) periodic solutions and examined their stability behavior. Remarkably, the system exhibited diverse bifurcation phenomena associated with pesticide-related parameters. Furthermore, the system demonstrated a multistability phenomenon involving the coexistence of the order-1 periodic solution and the limit cycle. This suggests that altering control strategies can disturb the initial coexistence status of pests and natural enemies. It also underscores that resource limitations can indeed impact the outbreak patterns and frequencies of pests. In addition to the variability in pesticide fatality rates, the inclusion of natural enemy releases in the nonlinear pulse strategy contributes to the model exhibiting complex dynamic characteristics. All these findings are substantiated by numerical simulations.

Keywords: Nonlinear pulse; State-dependent feedback control; Resource limitation; Fear effect; Anti-predator behavior; Order-k periodic solution

1 Introduction

Pest control [1, 2] involved the frequent occurrence of plant diseases and insect pests, the level of food quality and safety, and the maintenance of ecological civilization, and the sustainable development of the agricultural economy has been a major issue that has plagued people from ancient times to the present. The purpose of adhering to green prevention and control in the process of combating pests lies in reducing pesticide residues [3], increasing crop yield, and maintaining human health. Therefore pest control is a long-term and indispensable work of essential practical significance.

To efficiently control pest populations, an integrated Pest Management (IPM) strategy [4–7] emerged as a comprehensive approach in the field of pest control. Furthermore, mathematical models [8–11] were employed to illustrate the dynamics of fluctuations in the populations of pests and their natural enemies, with the renowned Lotka–Volterra (L-V) system being the most representative. Through years of development and exploration, various factors such as functional response [12, 13], nonsmooth control, and random perturbation [14] were considered to make relevant mathematical models more comprehensive and diverse, suitable for distinct pest control environments. These models enable us to conduct quantitative investigations into the effective reduction of pests, develop comprehensive and rational pest control strategies, and continually monitor pest populations in farmland to assess the efficacy of control measures.

The tenet of the IPM control strategy indicates that eradicating pests is unrealistic. The widespread approach is to limit the pest population to a certain state within the economic threshold ET [15]. Meanwhile, the economic harm level of pests can be ignored. Control measures, such as releasing natural enemies and spraying pesticides, should be implemented only when the pest population surpasses a certain threshold. Hence the unanimous consensus among scholars is the construction of a state-dependent pulse differential equation [12, 16–20] for Integrated Pest Management (IPM) strategies to examine the dynamic behavior of pest-natural enemy ecosystems.

In the actual process of pest control, many challenges are often more difficult than expected, and the impact of prey's anti-predator behavior [21–23], employed to resist predators and ensure self-security, on the system dynamics is one of them. The predators can suppress the prey in somatotype or attack means; the prey also constantly adapts to the environment to cope with the threat of the predators and reduce the risk of predation through camouflaging, burrowing, intimidating, and arranging sentries. For example, the ochotona curzoniae will reduce the time to go out to forage, and the wings of the vulnerable parus major grow faster to obtain the selective advantage of avoiding predators. Some prey even choose to actively attack young predators after discovering their nests to reduce their survival rate. Of course, counterattack also carries risks, known as the price or investment [24, 25] paid by prey in anti-predator behavior. In addition, the prey investment is inversely proportional to the number of predators.

The fear effect is another potential restraint form of predators against prey, in addition to predation, which is mainly reflected in the anxiety and timidity of prey due to fear of being eaten and leading to a decline in reproduction rate. Simultaneously, the fear effect can be interpreted as an alternative anti-predator behavior exhibited by prey. Prolonged fear may compel prey to seek refuge in caves, limiting their access to a broader habitat and hindering the accumulation of sufficient food reserves. Furthermore, this fear expands as the number of predators increases. Qi et al. [26] investigated a random predatory ecosystem incorporating fear effects and prey refuge. Their study demonstrated that mitigating predator fear and increasing the availability of shelters can enhance the survival rate of prey. Sarkar et al. [27] incorporated the fear effect into a predatory ecosystem with Holling II functional response. They observed that the alteration in prey growth rate caused by fear influenced the occurrence of Hopf bifurcation and altered its direction. This suggests that appropriately induced fear can lead to the stable coexistence of predators and prey. In addition, many meaningful biological conclusions have been proposed in [17, 21, 22, 28, 29], where the fear effect is considered.

Note that in the IPM strategy, the fatality rate of pesticides used for chemical control of pests is usually a constant [6, 30, 31], which is beneficial to facilitate the management and control of agricultural resources and monitor the actual situation of farmland. Actually, the effectiveness of pesticides will weaken with the increase of pest resistance. Furthermore, in the face of a large number of sudden and uncertain pest outbreaks, agricultural resources such as pesticides and manpower will be severely scarce. To cope with this sudden situation with limited resources [32, 33], an IPM strategy related to the nonlinear fatality rate amount depending on the state of pests is given, which is used to discuss the dynamic changes of the pest-natural enemy ecosystem with resource limitation. Qin et al. [34] investigated a predatory ecosystem with nonlinear pulse control. They employed sensitivity analysis to identify key factors influencing pest outbreaks and compared these findings with scenarios unaffected by resource limitations. The conclusion is drawn that improving the effectiveness of insecticides can more efficiently contain pests.

This paper is grounded in the concepts of resource limitations, fear effects, and anti-predator behavior. The objective is to formulate a state-dependent impulsive differential model that accurately captures the quantitative relationship between pests and natural enemies in farmland. Analyzing the stability of periodic solutions and investigating key parameters in nonlinear impulsive control are essential to assess the practical effectiveness of IPM control strategies. Special emphasis was placed on studying the outbreak patterns of pests, their influencing factors, and the threshold conditions required for the long-term coexistence of prey and predators.

The remainder of the paper is structured as follows. In the next section, we construct a nonsmooth predator–prey ecosystem with Holling II functional response. Section 3 delves into the fundamental properties of equilibrium points in the relevant Ordinary Differential Equation (ODE) model by exploring the connection between eigenvalues and the stability of planar systems. In Sect. 4, we present the pulse set and phase set under different thresholds and the definition and properties of the Poincaré map. In Sect. 5, we derive the necessary conditions for the stability of periodic solutions and validate the accuracy of these results through numerical simulation. The concluding section summarizes the key findings of the paper, unveiling the effectiveness of nonlinear pulse control.

2 Mathematical model

Based on a predator–prey two-dimensional planar system, the model is developed through the following steps:

(I) In 1987, Ives et al. [24] constructed a predator–prey ecological system with a functional response function:

$$\begin{cases} \frac{dx(t)}{dt} = rx(1-\frac{x}{K}) - v - \frac{e^{-\varepsilon v}qxy}{1+bx}, \\ \frac{dy(t)}{dt} = \frac{ce^{-\varepsilon v}qxy}{1+bx} - my. \end{cases}$$

(II) Take into account the influence of the fear effect on pests. Consequently, the first equation of the aforementioned model is modified to

$$\frac{dx(t)}{dt} = \frac{r}{1+ay}x\left(1-\frac{x}{K}\right) - v - \frac{e^{-\varepsilon v}qxy}{1+bx}.$$

Table 1 List of biological significance and dimensions

Parameters	Biological significance	Dimension
x	Pest population density	biomass
y	Predator population density	biomass
r	Maximum intrinsic growth rate of pests	time^{-1}
a	Cost of fear of predators	biomass^{-1}
K	Carrying capacity of the pest population	biomass
v	Investment of pests in anti-predator behavior	$\text{biomass} \cdot \text{time}^{-1}$
ε	Efficiency of the anti-predator behavior	$\text{biomass}^{-1} \cdot \text{time}$
q	Predation rate against pests	$\text{biomass}^{-1} \cdot \text{time}^{-1}$
b	Rate of predator satisfaction to prey	biomass^{-1}
c	Conversion rate of pests to predators	dimensionless
m	Mortality rate of predators	time^{-1}
p	Maximum instantaneous killing rate of a pesticide against pests	dimensionless
h	Half-saturation coefficient	biomass
τ	Maximum number of natural enemies released at one-time	biomass
δ	Tuning parameters for predator density	biomass^{-1}

Note that dimensionless means that the parameter cannot be represented by biomass and time in model (1). We refer to [35] for more information on the dimensions of parameters.

(III) In consideration of the agricultural economy, coupled with resource limitations, a nonlinear pulse control strategy is introduced. When the pest population reaches the threshold ET, actions such as pesticide spraying and natural enemy release are implemented, causing an instantaneous change in both pest and natural enemy numbers. This is described by the following continuous function:

$$I : \left(ET^{+}, y^{+}\right) = \left(\left[1 - \frac{pET}{ET + h}\right]ET, y(t) + \frac{\tau}{1 + \delta y(t)}\right).$$

Incorporating all the aforementioned factors, we derive the pulse semidynamic system:

$$\begin{cases} \left.\begin{aligned} \frac{dx(t)}{dt} &= \frac{r}{1+ay}x(1 - \frac{x}{K}) - v - \frac{e^{-\varepsilon v}qxy}{1+bx}, \\ \frac{dy(t)}{dt} &= \frac{ce^{-\varepsilon v}qxy}{1+bx} - my, \end{aligned}\right\} & x < ET, \\ \left.\begin{aligned} x(t^{+}) &= [1 - \frac{px(t)}{x(t)+h}]x(t), \\ y(t^{+}) &= y(t) + \frac{\tau}{1+\delta y(t)}, \end{aligned}\right\} & x = ET. \end{cases} \tag{1}$$

For a more convenient understanding of model (1), in Table 1, we list the biological significance and dimensions of all parameters in model (1).

In model (1) the applied pest control strategy comprises two components: intermittent pesticide spraying and the release of natural enemies. Typically, these two actions are carried out simultaneously. Due to resource constraints, it is imperative to minimize the depletion of the natural enemy population. Hence the chosen pesticide exclusively targets pests and has no impact on natural enemies. The pulse fluctuation in natural enemy density is solely attributable to the release quantity of natural enemies bred or acquired on the farm. For the model, we also see the proposal of $[1 - \frac{px(t)}{x(t)+h}]x(t)$, which suggests that the instantaneous killing rate of insecticides is not constant but rather a saturation function solely determined by the pest density at time $x = ET$. Likewise, the natural enemy release quantity is also tied to the current density of natural enemies. From this we can see that p and τ are the maximum killing rate and maximum release amount that combine the actual situation of farmland and resource limitation. Additionally, ε and v are

relevant parameters for anti-predation behavior, and we can see that the higher values of ε and ν resulting in lower predation rates.

Model (1) is based on the state feedback control model, taking into account both the fear effect and nonlinear impulse control term, and we used new qualitative analysis techniques and methods to study the properties of the semitrivial and order-1 periodic solution of model (1), established a threshold condition ensuring global stability of the periodic solution, revealed its underlying biological significance and conclusions, and proposed new ideas and strategies for reasonable comprehensive pest control.

3 Basic properties of an ODE model

To investigate the dynamic characteristics of the pest control model (1), we study the following model:

$$\begin{cases} \frac{dx(t)}{dt} = \frac{r}{1+ay}x(1-\frac{x}{K}) - \nu - \frac{e^{-\varepsilon\nu}qxy}{1+bx}, \\ \frac{dy(t)}{dt} = \frac{ce^{-\varepsilon\nu}qxy}{1+bx} - my. \end{cases} \tag{2}$$

Set the two equations of the above model equal to 0 and note the positivity of y. Therefore the two isoclines of the model (2) are

$$\begin{aligned} L_1: \quad & y = \frac{\sqrt{(a\nu + dqx + abvx)^2 + 4adqx(1+bx)(rx(1-\frac{x}{K}) - \nu)} - (a\nu + dqx + abvx)}{2adqx}, \\ L_2: \quad & \frac{cdqx}{1+bx} - m = 0, \end{aligned} \tag{3}$$

where $d = e^{-\varepsilon\nu}$. Obviously, when $y = 0$, model (2) has two boundary equilibria points $E_1(x_1, 0)$ and $E_2(x_2, 0)$, as illustrated in Fig. 1(A), and x_1 and x_2 are the two roots of equation $-rx^2 + Krx - K\nu = 0$,

$$x_1 = \frac{Kr - \sqrt{K^2r^2 - 4Kr\nu}}{2r} \quad \text{and} \quad x_2 = \frac{Kr + \sqrt{K^2r^2 - 4Kr\nu}}{2r}.$$

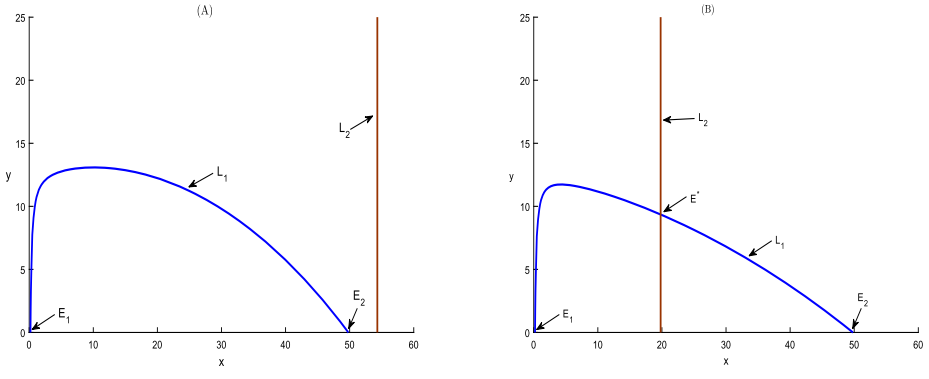

Figure 1 Position of equilibrium point, (*A*) and (*B*) are the cases where two isoclinic lines do not intersect and have intersections, respectively

We can see that y is positive when x is in the interval (x_1, x_2). Additionally, to ensure that both boundary equilibrium points are on the positive x-axis, the parameter ν meets $\nu < \frac{Kr}{4}$. On the other hand, according to the Vieta theorem, $x_1 + x_2 = K$.

When $y \neq 0$, we achieve the internal equilibrium point $E^*(x^*, y^*)$ with $x^* = \frac{m}{cdq-mb}$, as shown in Fig. 1(B). Substitute x^* into L_1 and make $cdq - mb = l$ to obtain

$$y^* = \frac{\sqrt{(avc+m)^2 + 4amc(r\frac{m}{l}(1-\frac{m}{Kl}) - \nu)} - (avc+m)}{2am}.$$

To demonstrate that the equilibrium $E^*(x^*, y^*)$ resides in the first quadrant, there is $cdq - mb > 0$, and both conditions $x_1 < x^* < x_2$ and $\nu < \frac{Kr}{4}$ mentioned above must be met. Otherwise, the two isoclinic lines of model (2) will not intersect in the first quadrant. To make the subsequent calculations more concise, we denote

$$\gamma = \sqrt{(avc+m)^2 + 4amc\left(r\frac{m}{l}\left(1-\frac{m}{Kl}\right) - \nu\right)} - (avc+m).$$

Therefore the internal equilibrium can be written as $E^*(\frac{m}{l}, \frac{\gamma}{2am})$.

When $a = 0$, that is, without considering the fear effect, model (2) can be expressed as

$$\begin{cases} \frac{dx(t)}{dt} = rx(1-\frac{x}{K}) - \nu - \frac{e^{-\varepsilon\nu}qxy}{1+bx}, \\ \frac{dy(t)}{dt} = \frac{ce^{-\varepsilon\nu}qxy}{1+bx} - my. \end{cases} \tag{4}$$

The establishment process and dynamic behavior of model (4) are presented in [24]. When $a = \nu = 0$, the fear effect and anti-predator factor are not involved. Hence model (2) can be written as

$$\begin{cases} \frac{dx(t)}{dt} = rx(1-\frac{x}{K}) - \frac{qxy}{1+bx}, \\ \frac{dy(t)}{dt} = \frac{cqxy}{1+bx} - my. \end{cases} \tag{5}$$

The dynamic characteristics of model (5) have been investigated in [12].

Therefore this paper is a further deepening of existing research, embodying the combination of anti-predator factor, Holling II functional response, and fear effect. A more detailed description of the pest-natural enemy ecosystem and a more rich population dynamic behavior is reflected.

In the following research, under the premise that both a and ν are not zero, the type and stability of the equilibrium are influenced by the real part symbol of characteristic value of the variational matrix constructed by the two-dimensional system. It should be emphasized that the numerical simulation at the end of the paper reveals that the value of x_1 is quite small. Therefore it is not in line with the actual biological situation where the number of pests is less than x_1. Hence we do not consider the case of $x^* < x_1$,

Theorem 1 *The stability conclusion of equilibrium points for system* (2).

(i) *When $x^* > x_2$, there is no internal equilibrium point in model* (2). *The boundary equilibrium point E_2 is stable, and E_1 is unstable.*

(ii) *When $x^* \in (x_1, x_2)$, if $\lambda < 0$ and $\Delta > 0$, then E^* is a stable node.*

(iii) *When* $x^* \in (x_1, x_2)$, *if* $\lambda < 0$ *and* $\Delta < 0$, *then* E^* *is a stable focus.*

(iv) *If* $cdqx_2/(1 + bx_2) - m > 0$ *and* $\lambda > 0$, *then* E^* *is deemed unstable, and model* (2) *exhibits precisely one stable limit cycle in the first quadrant.*

Here λ *and* Δ *are defined in the proof.*

Proof System (2) can be regarded as the differential equation system

$$\begin{cases} \frac{dx(t)}{dt} = P(x, y), \\ \frac{dy(t)}{dt} = Q(x, y), \end{cases}$$

and the variational matrix of system (2) is

$$\begin{aligned} J(x, y) &= \begin{pmatrix} \frac{\partial P}{\partial x} & \frac{\partial P}{\partial y} \\ \frac{\partial Q}{\partial x} & \frac{\partial Q}{\partial y} \end{pmatrix} \\ &= \begin{pmatrix} \frac{r}{1+ay} - \frac{2r}{K(1+ay)}x - \frac{dqy}{(1+bx)^2} & -\frac{arx(1-\frac{x}{K})}{(1+ay)^2} - \frac{dqx}{1+bx} \\ \frac{cdqy}{(1+bx)^2} & \frac{cdqx}{1+bx} - m \end{pmatrix}. \end{aligned} \tag{6}$$

Substituting the equilibrium point $E_1(x_1, 0)$ into matrix (6) yields

$$J|_{E_1} = \begin{pmatrix} r - \frac{2r}{K}x_1 & -arx_1(1 - \frac{x_1}{K}) - \frac{dqx_1}{1+bx_1} \\ 0 & \frac{cdqx_1}{1+bx_1} - m \end{pmatrix}.$$

By calculating we have $r - \frac{2r}{K}x_1 = \frac{\sqrt{K^2r^2 - 4Krv}}{K} > 0$. Therefore the positivity of trace and determinant of a matrix $J|_{E_1}$ depend on $\frac{cdqx_1}{1+bx_1} - m$. For this purpose, it is advisable to define

$$\rho(x) = \frac{cdqx}{1 + bx} - m.$$

Differentiating $\rho(x)$, we have

$$\rho'(x) = \frac{cdq}{(1 + bx)^2} > 0$$

for $x > 0$. Hence $\rho(x)$ is increasing with respect to x. Note that when $x = x^*$, we have $\rho(x^*) = 0$. For $x_1 < x^*$, we have $\rho(x_1) < 0$, and thus

$$\det J|_{E_1} = \left(r - \frac{2r}{K}x_1\right)\left(\frac{cdqx_1}{1 + bx_1} - m\right) < 0,$$

which shows that E_1 is a saddle.

Similarly, substituting E_2 into matrix (6) yields

$$J|_{E_2} = \begin{pmatrix} r - \frac{2r}{K}x_2 & -arx_2(1 - \frac{x_2}{K}) - \frac{dqx_2}{1+bx_2} \\ 0 & \frac{cdqx_2}{1+bx_2} - m \end{pmatrix}.$$

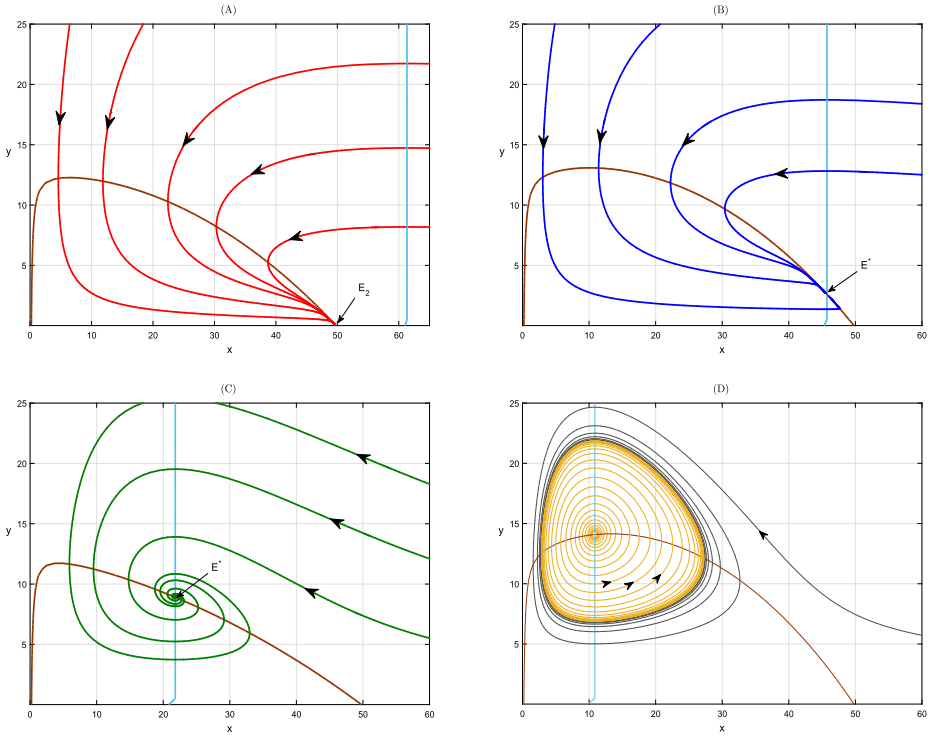

Figure 2 The dynamics of system (2) under cases (i)–(iv). The parameters are $r = 2$, $K = 50$, $q = 0.2$, $a = 0.005$, $c = 0.5$, $v = 0.4$, $\varepsilon = 0.8$. (A) $m = 2$, $b = 0.02$; (B) $m = 1.4$, $b = 0.03$; (C) $m = 1.3$, $b = 0.01$; (D) $m = 0.55$, $b = 0.04$

By calculating we have $r - \frac{2r}{K}x_2 = -\frac{\sqrt{K^2r^2-4Krv}}{K} < 0$. Just like above, for $x_2 < x^*$, we obtain $\rho(x_2) < 0$. Hence

$$\begin{aligned}
\operatorname{tr} J|_{E_2} &= \left(r - \frac{2r}{K}x_2\right) + \left(\frac{cdqx_2}{1+bx_2} - m\right) < 0,\\
\det J|_{E_2} &= \left(r - \frac{2r}{K}x_2\right)\left(\frac{cdqx_2}{1+bx_2} - m\right) > 0,
\end{aligned}$$

which means that E_2 is a stable node or focus, as illustrated in Fig. 2(A).

Analogously, substituting E^* into matrix (6) yields

$$J|_{E^*} = \begin{pmatrix} \frac{2Klrm-4rm^2}{Kl(2m+\gamma)} - \frac{l^2\gamma}{2ac^2dqm} & \frac{-4arm^3(Kl-m)}{Kl^2(2m+\gamma)^2} - \frac{m}{c} \\ \frac{l^2\gamma}{2acdqm} & 0 \end{pmatrix}.$$

To determine the stability of E^*, we define

$$\begin{aligned}
\eta = \det J|_{E^*} &= -\left(\frac{-4arm^3(Kl-m)}{Kl^2(2m+\gamma)^2} - \frac{m}{c}\right)\left(\frac{l^2\gamma}{2acdqm}\right)\\
&= \frac{4acrm^2\gamma(Kl-m) + Kl^2\gamma(2m+\gamma)^2}{2ac^2dqK(2m+\gamma)^2},\\
\lambda = \operatorname{tr} J|_{E^*} &= \frac{2Klrm-4rm^2}{Kl(2m+\gamma)} - \frac{l^2\gamma}{2ac^2dqm},
\end{aligned}$$

$$\Delta = disc J|_{E^*} = \lambda^2 - 4\eta.$$

Here Δ is the discriminant of the characteristic equation of $J|_{E^*}$. According to (6), we can see that $\eta > 0$. Therefore, based on the relationship between equilibrium points and eigenvalues, we can conclude that when $\lambda < 0$ and $\Delta > 0$, the equilibrium point E^* represents a stable node, as depicted in Fig. 2(B); when $\lambda < 0$ and $\Delta < 0$, the equilibrium point E^* becomes a stable focus, as illustrated in Fig. 2(C). Specifically, if $\lambda > 0$, then E^* is unstable. Hence the existence of a limit cycle can be established based on the Poincaré–Bendixson theorem [36, 37], which states that when the equilibrium points E_2 and E^* are unstable, i.e., under the assumptions $\frac{cdqx_2}{1+bx_2} - m > 0$ and $\lambda > 0$, system (2) possesses precisely one limit cycle in the first quadrant, as illustrated in Fig. 2(D). □

4 Poincaré map

To analyze the global dynamics of system (1) using the Poincaré map, it is essential to delineate the extent of the phase set. To achieve this, we need a combination of a phase diagram and the value of ET.

4.1 Pulse set

To demonstrate the biological significance of the model, define the valid range $R^2 = \{(x,y)|x \geq 0, y \geq 0\}$ to ensure that the populations of pests and natural enemies consistently fall within this range. Additionally, considering the constraint $ET < K$, define the set

$$\Lambda = \{(x,y)|0 < x < ET, y > 0\} \subset R^2.$$

Now, according to the part where $x = ET$ in system (1), we can also define it as follows:

$$L_3: \quad x = (1-\theta)ET, \qquad L_4: \quad x = ET.$$

Here $\theta = \frac{pET}{ET+h}$ and $0 \leq \theta < 1$. For the convenience of writing, equation (3) can be written as

$$L_1: \quad y = g(x).$$

Hence the intersection of L_1 and L_3 can be defined as $Q_0 = ((1-\theta)ET, y_{Q_0})$, where

$$y_{Q_0} = g\big((1-\theta)ET\big).$$

Analogously, we can obtain the intersection point of L_1 and L_4, denoted as $T = (ET, y_T)$, where

$$y_T = g(ET).$$

Note that for system (1), $0 \leq y \leq y_T$ represents the maximum range of the ordinate in the pulse set. Therefore the pulse set obtained is

$$\mathcal{M} = \{(x,y) \in R^2 | x = ET, 0 \leq y \leq y_T\}.$$

Obviously, $\mathcal{M}$ is included within R^2. With the function $I:(x,y)\to(x^+,y^+)$, where (x^+,y^+) denotes an impulsive point corresponding to (x,y), the phase set is defined as

$$\mathcal{N}=I(\mathcal{M})=\left\{\left(x^+,y^+\right)\in\Lambda\,|x^+=(1-\theta)ET,y^+\in Y_0\right\},$$

where the range of Y_0 depends on the monotonicity of the nonmonotonic term $\frac{\tau}{1+\delta y(t)}$. It will be a focal point in our subsequent investigation into the precise boundaries of the phase set. Unless specified otherwise, we assume that the initial values (x_0^+,y_0^+) belong to $\mathcal{N}$.

According to Theorem 1, we implement the following classification.

$$\text{Case (i):}\quad H_1:\quad ET\le x_2,\qquad H_2:\quad ET>x_2. \tag{7}$$

$$\text{Case (ii):}\quad I_1:\quad ET\le x^*,\qquad I_2:\quad ET>x^*. \tag{8}$$

$$\text{Case (iii):}\quad J_1:\quad ET\le x^*,\qquad J_2:\quad ET>x^*\begin{cases}J_{21}:\quad (1-\theta)ET<x_3,\\ J_{22}:\quad (1-\theta)ET\ge x_3.\end{cases} \tag{9}$$

$$\text{Case (iv):}\quad \begin{aligned}&K_1:\quad ET\le x^*,\qquad K_2:\quad ET\ge x_5\begin{cases}K_{21}:\quad (1-\theta)ET<x_3,\\ K_{22}:\quad (1-\theta)ET\ge x_3,\end{cases}\\ &K_3:\quad x^*<ET<x_5\begin{cases}K_{31}:\quad (1-\theta)ET\le x_4,\\ K_{32}:\quad (1-\theta)ET>x_4.\end{cases}\end{aligned} \tag{10}$$

Here x_3, x_4, and x_5 are defined in the proof of Lemma 2.

Lemma 2 *When ET and $(1-\theta)ET$ meet conditions (7)–(10), respectively, the corresponding pulse set obtained is as follows*:

$$\mathcal{M}_\times\begin{cases}H_2,\\ I_2.\end{cases}\qquad \mathcal{M}\begin{cases}J_{22},\\ K_{22},\\ K_{32}.\end{cases}\qquad \mathcal{M}_1\begin{cases}H_1,I_1,\\ J_1,J_{21},\\ K_1,K_{21},K_{31}.\end{cases}$$

Here $\mathcal{M}_\times$ indicates that the pulse set of these cases cannot be defined and the pulse set

$$\mathcal{M}_1=\left\{(x,y)\in R^2|x=ET,0\le y\le y_{Q_1}\right\},$$

where y_{Q_1} is the ordinate of the intersection point between the curve tangent to L_3 and line L_4.

Proof For Case (i), as shown in Fig. 3, there is no internal equilibrium point in system (1), and all solutions tend to be stable E_2. Then there must be a trajectory tangent to L_3, denoted as Γ_1, with a tangent point of Q_0. As both ET and x_2 are less than K, it is imperative to explore the relationship between ET and x_2. If $ET\le x_2$, then the intersection of Γ_1 and line L_4 is defined as Q_1. Therefore the pulse set is $\mathcal{M}_1$. If $ET>x_2$, then we cannot determine whether the trajectory of system (1) intersects with line L_4, and thus we are unable to provide an accurate domain of the pulse set.

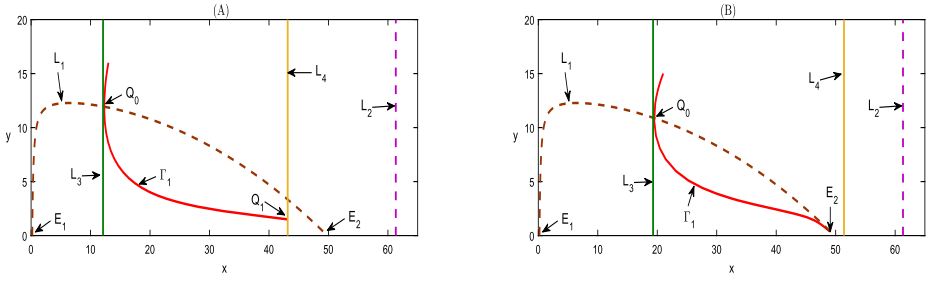

Figure 3 Pulse set for Case (i). (A) Subcase H_1; (B) Subcase H_2. The parameters are the same as in Fig. 2(A)

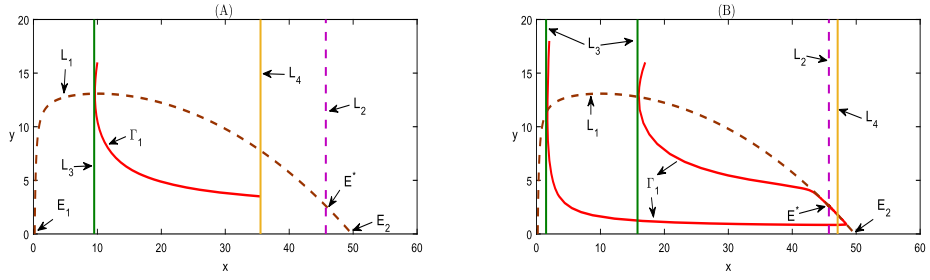

Figure 4 Pulse set for Case (ii). (A) Subcase I_1; (B) Subcase I_2. The parameters are the same as in Fig. 2(B)

For Case (ii), as shown in Fig. 4, consistent with the analysis method of case H_1, if $ET \leq x^*$, then the pulse set is $\mathcal{M}_1$. If $ET > x^*$, then the curve originating from the phase set will converge to a stable node E^* along the asymptotic line, which may not reach the pulse set, so the accurate domain of the pulse set cannot be given.

According to Fig. 5, we can seen that for subcase J_1 in Case (iii), like in case H_1, the pulse set is $\mathcal{M}_1$. For J_2, when $ET > x^*$, there must be a trajectory tangent to L_4, denoted as Γ_2, with a tangent point of T. In addition, the point T is also one of the two intersections of Γ_2 and L_1, and the other intersection point is defined as E_3. If $(1-\theta)ET < x_3$, then as in case H_1, the pulse set is $\mathcal{M}_1$. If $(1-\theta)ET \geq x_3$, then there will be two intersections of L_3 and trajectory Γ_2. The point with a larger ordinate will be denoted P_1, and the other point will be denoted P_2. Obviously, except for the points between P_2 and P_1, all trajectories starting from L_3 can reach the set $\mathcal{M}$.

In Case (iv), as depicted in Fig. 6, there exists a limit cycle in model (1), denoted Ω, then Ω and L_1 will have left and right intersections, denoted E_4 and E_5, respectively. According to the relationship of x^*, x_5 and ET, consider the three cases of K_1, K_2, and K_3. For cases K_1 and K_{31}, like in case H_1, the pulse set is $\mathcal{M}_1$. For subcases K_{21} and K_{22} in case K_2, as in cases J_{21} and J_{22}, the pulse sets are $\mathcal{M}_1$ and $\mathcal{M}$, respectively. For case K_{32}, when $x^* < ET < x_5$ and $(1-\theta)ET > x_4$, any solution starting from L_3 either directly reaches the pulse set, or there will be many intersections with L_3 before reaching the pulse set. Hence the pulse set is $\mathcal{M}$.

Note that when L_3 and L_2 coincide, E^* cannot be used as the initial point. □

Note that in many cases, the definition of pulse sets needs to be analyzed in conjunction with phase sets, and we will focus on examining them in the next section.

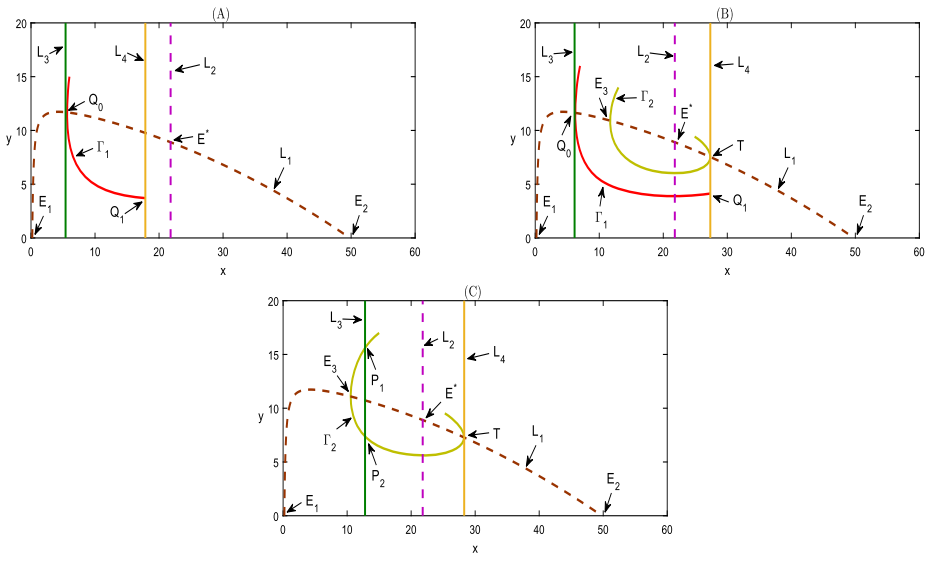

Figure 5 Pulse set for Case (iii). (A) Subcase J_1; (B) Subcase J_{21}; (C) Subcase J_{22}. The parameters are the same as in Fig. 2(C)

4.2 Phase set

According to the definition of a pulse set for classification conditions (7)–(10) and above, we found that the dynamics of the solution trajectory starting from phase set $\mathcal{N}$ exhibit multiple possibilities. Hence, to define the phase set under different conditions and examine the characteristics of periodic solutions using the Poincaré map on the phase set, it is crucial to identify the specific range where the solution of system (1) starting from the phase set remains unaffected by impulsive effects. This observation is evident in Fig. 5(C) and Fig. 6(C), where any solution originating from the section line $\overline{P_1P_2}$ is devoid of pulse effects. For these two cases, we define the set

$$Y_{is} = [0, y_{P_2}] \cup [y_{P_1}, +\infty],$$

where y_{P_1} and y_{P_2} are the ordinates of points P_1 and P_2, respectively. To investigate the impact of the nonmonotonic term $y(t) + \frac{\tau}{1+\delta y(t)}$ on the dynamics of system (1), define the pulse function

$$f(y) = y + \frac{\tau}{1 + \delta y}. \tag{11}$$

Differentiating equation (11), we obtain

$$f'(y) = 1 - \frac{\tau\delta}{(1 + \delta y)^2}.$$

Solving $f'(y) = 0$, we get $y = \frac{\sqrt{\tau\delta}-1}{\delta}$. By calculation we obtain that if $y > \frac{\sqrt{\tau\delta}-1}{\delta}$, then the function $f(y)$ is increasing, and if $y < \frac{\sqrt{\tau\delta}-1}{\delta}$, then the function $f(y)$ is decreasing. For analyzing the phase set, we need the following lemma.

Lemma 3 *If the pulse set is the same, then the phase set is the same.*

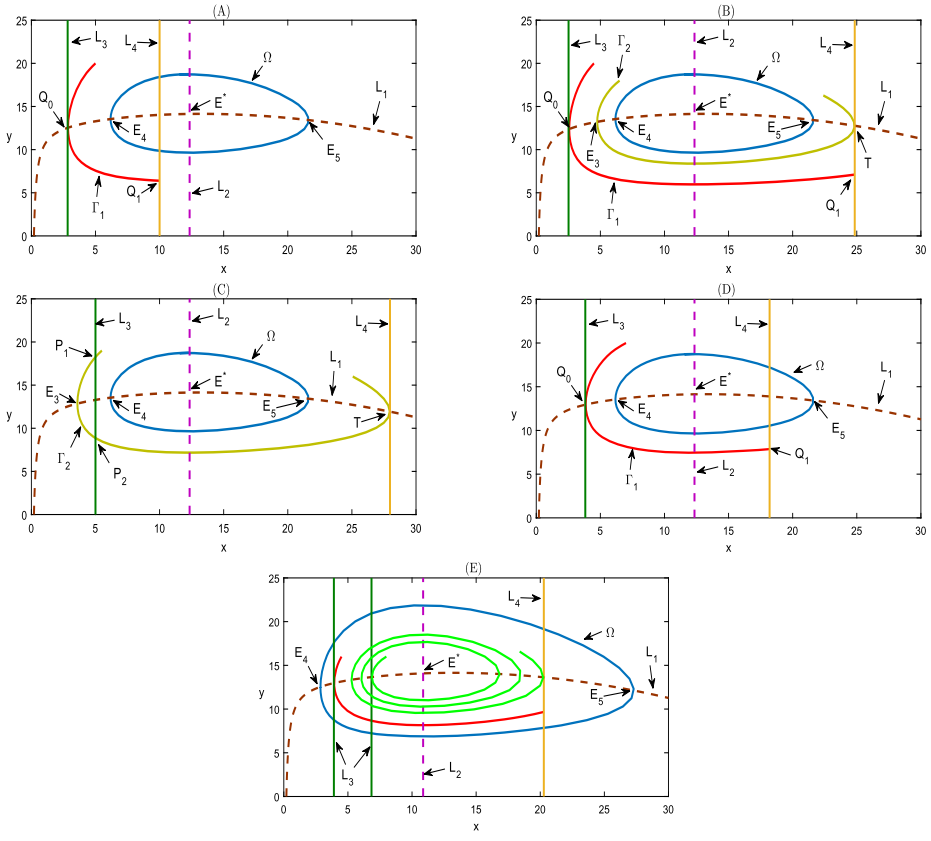

Figure 6 Pulse set for case (iv). (A) Subcase K_1; (B) Subcase K_{21}; (C) Subcase K_{22}; (D) Subcase K_{31}; (E) Subcase K_{32}. Except for $m = 2$ in subfigure (E), all other parameters are the same as in Fig. 2(D)

Proof In a specific case, for $\mathcal{N} = I(\mathcal{M})$, we can see that the abscissa of a point (x, y) in M is always mapped from ET to $(1 - \theta)ET$, and the ordinate is mapped from y to $f(y)$ after the action of function I. Therefore the phase set is determined by the pulse set and the pulse function. This correspondence is just like the range is calculated according to the analytic expression and the domain. Therefore the phase set is the same when the pulse set is the same. □

For the pulse set $\mathcal{M}_1$, the domain of y is $[0, y_{Q_1}]$. Because the monotonicity of the pulse function (11) varies in different intervals, the following three subcases are analyzed.

(a) If $\frac{\sqrt{\tau\delta}-1}{\delta} \leq 0$, then it is not difficult to get that the pulse function $f(y)$ is increasing on the interval $[0, y_{Q_1}]$, indicating that

$$\tau = f(0) \leq f(y) \leq f(y_{Q_1}) = y_{Q_1} + \frac{\tau}{1 + \delta y_{Q_1}}.$$

So define the set

$$Y_1 = \left[\tau, y_{Q_1} + \frac{\tau}{1 + \delta y_{Q_1}}\right].$$

Therefore, in this case, the phase set corresponding to the pulse set $\mathcal{M}_1$ is

$$\mathcal{N}_1 = \left\{\left(x^+, y^+\right) \in \Lambda \,|\, x^+ = (1-\theta)ET, y^+ \in Y_1\right\}.$$

(b) If $\frac{\sqrt{\tau\delta}-1}{\delta} \geq y_{Q_1}$, then the pulse function $f(y)$ is decreasing on the interval $[0, y_{Q_1}]$, indicating that

$$y_{Q_1} + \frac{\tau}{1+\delta y_{Q_1}} = f(y_{Q_1}) \leq f(y) \leq f(0) = \tau.$$

So define the set

$$Y_2 = \left[y_{Q_1} + \frac{\tau}{1+\delta y_{Q_1}}, \tau\right].$$

Therefore, in this case, the phase set corresponding to the pulse set $\mathcal{M}_1$ is

$$\mathcal{N}_2 = \left\{\left(x^+, y^+\right) \in \Lambda \,|\, x^+ = (1-\theta)ET, y^+ \in Y_2\right\}.$$

(c) If $0 < \frac{\sqrt{\tau\delta}-1}{\delta} < y_{Q_1}$, then the function $f(y)$ is decreasing on the interval $[0, \frac{\sqrt{\tau\delta}-1}{\delta}]$ and increasing on the interval $(\frac{\sqrt{\tau\delta}-1}{\delta}, y_{Q_1}]$, with $f(\frac{\sqrt{\tau\delta}-1}{\delta}) = \frac{2\sqrt{\tau\delta}-1}{\delta}$ being the minimum value on the interval $[0, y_{Q_1}]$, and the maximum value is $f(0)$ or $f(y_{Q_1})$. Hence we define the interval

$$Y_3 = \left[\frac{2\sqrt{\tau\delta}-1}{\delta}, y_\tau^1\right], \quad y_\tau^1 = \max\left\{\tau, y_{Q_1} + \frac{\tau}{1+\delta y_{Q_1}}\right\}.$$

Therefore, in this case, the phase set corresponding to the pulse set $\mathcal{M}_1$ is

$$\mathcal{N}_3 = \left\{\left(x^+, y^+\right) \in \Lambda \,|\, x^+ = (1-\theta)ET, y^+ \in Y_3\right\}.$$

According to Lemma 3, the phase sets of cases H_1, I_1, J_1, J_{21}, K_1, K_{21}, and K_{31} can all be defined in this way.

For the pulse set $\mathcal{M}$, the domain of y is $[0, y_T]$. Considering the monotonicity of the pulse function and the fact that the solution trajectory starting from within section line $\overline{P_1P_2}$ will not experience pulse effects, we analyze the following three subcases.

(d) If $\frac{\sqrt{\tau\delta}-1}{\delta} \leq 0$, then the pulse function $f(y)$ is increasing on the interval $[0, y_T]$, indicating that

$$\tau = f(0) \leq f(y) \leq f(y_T) = y_T + \frac{\tau}{1+\delta y_T}.$$

So define the set

$$Y_4 = Y_{41} \cap Y_{is}, \quad Y_{41} = \left[\tau, y_T + \frac{\tau}{1+\delta y_T}\right].$$

Therefore, in this case, the phase set is

$$\mathcal{N}_4 = \left\{\left(x^+, y^+\right) \in \Lambda \,|\, x^+ = (1-\theta)ET, y^+ \in Y_4\right\}.$$

Table 2 Impulsive and phase sets of system (1)

Case		ET	$(1-\theta)ET$	$\mathcal{M}_s$	$\mathcal{N}_s$
	(a)				$\mathcal{N}_1$
J_{21}	(b)	$ET > x^*$	$(1-\theta)ET < x_3$	$\mathcal{M}_1$	$\mathcal{N}_2$
	(c)				$\mathcal{N}_3$
	(d)				$\mathcal{N}_4$
J_{22}	(e)	$ET > x^*$	$(1-\theta)ET \geq x_3$	$\mathcal{M}$	$\mathcal{N}_5$
	(f)				$\mathcal{N}_6$

(e) If $\frac{\sqrt{\tau\delta}-1}{\delta} \geq y_T$, then the pulse function $f(y)$ is decreasing on the interval $[0, y_T]$, indicating that

$$y_T + \frac{\tau}{1+\delta y_T} = f(y_T) \leq f(y) \leq f(0) = \tau.$$

So define the set

$$Y_5 = Y_{51} \cap Y_{is}, \quad Y_{51} = \left[y_T + \frac{\tau}{1+\delta y_T}, \tau \right].$$

Therefore, in this case, the phase set is

$$\mathcal{N}_5 = \left\{ \left(x^+, y^+\right) \in \Lambda \,|\, x^+ = (1-\theta)ET, y^+ \in Y_5 \right\}.$$

(f) If $0 < \frac{\sqrt{\tau\delta}-1}{\delta} < y_T$, then the function $f(y)$ is decreasing on the interval $[0, \frac{\sqrt{\tau\delta}-1}{\delta}]$ and increasing on the interval $(\frac{\sqrt{\tau\delta}-1}{\delta}, y_T]$, with $f(\frac{\sqrt{\tau\delta}-1}{\delta}) = \frac{2\sqrt{\tau\delta}-1}{\delta}$ being the minimum value on interval $[0, y_T]$, and the maximum value is $f(0)$ or $f(y_T)$. Hence we define the interval

$$Y_6 = Y_{61} \cap Y_{is}, \quad Y_{61} = \left[\frac{2\sqrt{\tau\delta}-1}{\delta}, y_\tau^2 \right], \quad y_\tau^2 = \max\left\{ \tau, y_T + \frac{\tau}{1+\delta y_T} \right\}.$$

Therefore, in this case, the phase set is

$$\mathcal{N}_6 = \left\{ \left(x^+, y^+\right) \in \Lambda \,|\, x^+ = (1-\theta)ET, y^+ \in Y_6 \right\}.$$

According to Lemma 3, the phase sets of cases J_{22}, K_{22}, and K_{32} can all be defined in this way.

For the pulse set $\mathcal{M}_\times$, since the domain of y cannot be determined, an accurate phase set cannot be obtained. Therefore, for cases H_2 and I_2, we define the phase set as $\mathcal{N}_\times$.

The monotonicity of the nonlinear pulse function and the diversity of ET selection can cause the system to exhibit various complex dynamics. Therefore we select two representative cases J_{21} and J_{22} for analysis. To summarize the above discussion, we list the selected cases in Table 2.

4.3 Establishment of Poincaré map

Given the properties of the successor function, we can provide a mathematical expression for the Poincaré map. Assuming that $p_k^+((1-\theta)ET, y_k^+)$ is a point belonging to the phase set, the solution $\psi(t, t_0, (1-\theta)ET, y_k^+)$ with an initial value of p_k^+ reaches the point $p_{k+1}(ET, y_{k+1})$ on the pulse set after time t_1. This indicates that the location of point p_{k+1} is influenced by

the coordinates of point p_k^+. Then $y_{k+1} = \mathcal{A}(y_k^+)$. The solution ψ of system (1) transitions to the point $p_{k+1}^+((1-\theta)ET, y_{k+1}^+)$ after a pulse effect at point p_{k+1}, where $y_{k+1}^+ = y_{k+1} + \frac{\tau}{1+\delta y_{k+1}}$. So the Poincaré map can be defined as

$$y_{k+1}^+ = f\big(\mathcal{A}(y_k^+)\big) = \mathcal{A}(y_k^+) + \frac{\tau}{1+\delta\mathcal{A}(y_k^+)} \doteq \varphi(y_k^+). \tag{12}$$

Since the function $\mathcal{A}(y_k^+)$ is continuously differentiable with respect to y_k^+, $\varphi(y_k^+)$ is also continuously differentiable with respect to y_k^+. Therefore the existence of a fixed point in $\varphi(y_k^+)$ is equivalent to the presence of an order-1 periodic solution within system (1).

Remark 4 If $\frac{\sqrt{\tau\delta}-1}{\delta}$ is the ordinate of a point on the pulse set, then define a key point $Q_\delta(x_{Q_\delta}, y_{Q_\delta}) = (ET, \frac{\sqrt{\tau\delta}-1}{\delta})$, and after the pulse effect, the corresponding pulse point is marked as $Q_\delta^+(x_{Q_\delta^+}, y_{Q_\delta^+}) = ((1-\theta)ET, \frac{2\sqrt{\tau\delta}-1}{\delta})$.

Theorem 5 *For cases J_{21} and J_{22}, we have the following properties of $\varphi(y_k^+)$:*

(i*) *For case J_{21}, system (1) has a stable focus, $ET > x^*$ and $(1-\theta)ET < x_3$, the monotonicity of $\varphi(y_k^+)$ is shown in the upper half of Table 3.*

(ii*) *For case J_{22}, system (1) has a stable focus, $ET > x^*$ and $(1-\theta)ET \geq x_3$, the monotonicity of $\varphi(y_k^+)$ is shown in the lower half of Table 3.*

(iii*) *If the point $p_k^+((1-\theta)ET, y_k^+)$ is the pulse point corresponding to the point $p_k(ET, y_k)$, and ζ_k is the slope of pulse segment $\overline{p_k^+ p_k}(k = 1, 2, 3, \ldots)$, then we conclude that if $y_{k+1} > y_k$, then $\zeta_{k+1} > \zeta_k$.*

(iv*) *$\varphi(y_k^+)$ has a horizontal asymptote $y = \tau$.*

Proof (i*) Based on the previous analysis, we easily get that the domain of $\varphi(y_k^+)$ is $[0, +\infty)$. For the three subcases of J_{21}, any solution curve originating from the interval $[0, +\infty)$ causes the pulse effect. By the motion trend of the vector field and the uniqueness of the solution the function $\mathcal{A}(y_k^+)$ increases on the interval $[0, y_{Q_0}]$ and decreases on the interval $(y_{Q_0}, +\infty)$. On the other hand, for subcase (a), the impulse function $f(y)$ increases within $[0, y_{Q_1}]$. According to the nature of composite function, $\varphi(y_k^+)$ increases within the interval

Table 3 Monotonicity of map $\varphi(y_k^+)$

Case	Interval	$\mathcal{A}(y_k^+)$	$f(y)$	$\varphi(y_k^+)$
J_{21}(a)	In	$[0, y_{Q_0}]$	$[0, y_{Q_1}]$	$[0, y_{Q_0}]$
	De	$(y_{Q_0}, +\infty)$	–	$(y_{Q_0}, +\infty)$
J_{21}(b)	In	$[0, y_{Q_0}]$	–	$(y_{Q_0}, +\infty)$
	De	$(y_{Q_0}, +\infty)$	$[0, y_{Q_1}]$	$[0, y_{Q_0}]$
J_{21}(c)	In	$[0, y_{Q_0}]$	$(\frac{\sqrt{\tau\delta}-1}{\delta}, y_{Q_1}]$	$(y_d, y_{Q_0}), (y_u, +\infty)$
	De	$(y_{Q_0}, +\infty)$	$[0, \frac{\sqrt{\tau\delta}-1}{\delta}]$	$[0, y_d], [y_{Q_0}, y_u]$
J_{22}(d)	In	$[0, y_{P_2}]$	$[0, y_T]$	$[0, y_{P_2}]$
	De	$[y_{P_1}, +\infty)$	–	$[y_{P_1}, +\infty)$
J_{22}(e)	In	$[0, y_{P_2}]$	–	$[y_{P_1}, +\infty)$
	De	$[y_{P_1}, +\infty)$	$[0, y_T]$	$[0, y_{P_2}]$
J_{22}(f)	In	$[0, y_{P_2}]$	$(\frac{\sqrt{\tau\delta}-1}{\delta}, y_T]$	$(y_D, y_{P_2}], (y_U, +\infty)$
	De	$[y_{P_1}, +\infty)$	$[0, \frac{\sqrt{\tau\delta}-1}{\delta}]$	$[0, y_D], [y_{P_1}, y_U]$

$[0, y_{Q_0}]$ and decreases within the interval $(y_{Q_0}, +\infty)$. The same analysis method is used for cases (b) and (c).

(ii*) For case J_{22}, note that the effective domain of $\varphi(y_k^+)$ is $[0, y_{P_2}] \cup [y_{P_1}, +\infty]$, and the rest of the reasoning process is consistent with (i*).

(iii*) When $x = ET$, the nonlinear term of system (1) leads to the nonparallelism of pulse segment $\overline{p_k^+ p_k}$ $(k = 1, 2, 3, \dots)$. When $\tau > 0$, the slope

$$\zeta_k = \frac{y_k^+ - y_k}{(1-\theta)ET - ET} = -\frac{\tau}{\theta ET(1+\delta y_k)} < 0.$$

On the other hand, considering ζ_k as a function of y_k and taking the derivative of ζ_k, we have $\zeta_k'(y_k) = \frac{\tau\delta}{\theta ET(1+\delta y_k)^2} > 0$. Therefore the slope ζ_k is increasing with respect to y_k, indicating that when $y_{k+1} > y_k$, we have $\zeta_{k+1} > \zeta_k$.

(iv*) To illustrate that map $\varphi(y_k^+)$ has a horizontal asymptote $y = \tau$, we need to establish the limit

$$\lim_{y_k^+ \to +\infty} \left(\mathcal{A}(y_k^+) + \frac{\tau}{1 + \delta \mathcal{A}(y_k^+)} \right) = \tau,$$

meaning that as $y_k^+ \to +\infty$, we have $\mathcal{A}(+\infty) = 0$, which can be explained by using reduction to absurdity. If $\mathcal{A}(+\infty) = y_* > 0$, then choose a point $P(ET, y_P)(0 < y_P < y_*)$. Then there must be a trajectory Γ between the x-axis and the trajectory where P is located, and Γ will intersect with L_3 at two points. The point above is defined as $P_0((1-\theta)ET, y_{P_0})$ based on the property of no intersection between any two solutions, which leads to $y_{P_0} > +\infty$, which is a contradiction. Therefore $\mathcal{A}(+\infty) = 0$. Hence $\varphi(y_k^+)$ has a horizontal asymptote $y = \tau$. □

5 Relevant properties of periodic solution

According to the above discussion, Table 2 reveals that the parameter θ, being a sensitive factor, plays a pivotal role in the derivation of Poincaré maps, analogous to the significance of ET. Now we will explore how the impact of these parameters on the periodic solution manifests in the dynamics of system (1).

5.1 Boundary order-1 periodic solution with $\tau = 0$

On the premise of not artificially releasing natural enemies, evidently, $\varphi(y_i^+)$ possesses a fixed point at $y = 0$. It suggests the presence of a first-order periodic solution along the boundary in system (1). Indeed, by treating $y(t)$ and τ in system (1) as 0, we can derive the subsystem

$$\begin{cases} \frac{dx(t)}{dt} = rx(1 - \frac{x}{K}) - v, & x < ET, \\ x(t^+) = [1 - \frac{px(t)}{x(t)+h}]x(t), & x = ET. \end{cases} \tag{13}$$

To ensure the normal operation of pulse measures, the value of x needs to increase from $(1-\theta)ET$ to ET, and then the inequality $\frac{dx}{dt} > 0$ is satisfied, which implies $v < \frac{Kr}{4}$. Additionally, based on the previous analysis, the value of x must satisfy $x_1 < x < x_2$. Hence the value of ET also satisfies $x_1 < (1-\theta)ET < ET < x_2$ with $\theta \neq 0$.

The equation at time $x < ET$ in model (13) can be rewritten as $\frac{dx}{dt} = -\frac{r}{K}(x - x_1)(x - x_2)$ and then converted into equation of separated variables

$$\frac{dx}{(x - x_1)(x - x_2)} = -\frac{r}{K}\,dt.$$

After performing the calculation, the solution to system (13) is

$$x = \frac{x_1 + x_2 Ce^{\xi t}}{1 + Ce^{\xi t}}, \quad \xi = \frac{r}{K}(x_2 - x_1) > 0. \tag{14}$$

By substituting the initial value $((1 - \theta)ET, 0)$ we obtain

$$C = \frac{(1 - \theta)ET - x_1}{x_2 - (1 - \theta)ET}. \tag{15}$$

After a cycle T, the number of x reaches ET. Hence

$$ET = \frac{x_1 + x_2 Ce^{\xi T}}{1 + Ce^{\xi T}}.$$

Using T as a variable, we calculate

$$T = \frac{1}{\xi} In \frac{[x_2 - (1 - \theta)ET](ET - x_1)}{[(1 - \theta)ET - x_1](x_2 - ET)}. \tag{16}$$

Therefore the solution of system (1) on the positive x-axis is

$$\left(x^T(t), 0\right) = \left(\frac{x_1 + x_2 Ce^{\xi t}}{1 + Ce^{\xi t}}, 0\right). \tag{17}$$

To demonstrate the asymptotic stability of solution (17), we utilize a Poincaré criterion analogy.

Theorem 6 *Under the condition*

$$\sigma^{-\frac{1}{x_2 - x_1}\left(\frac{Km}{r} - \frac{cdqKx_1}{r(1 + bx_1)}\right)} < \left(\frac{\vartheta + C}{\vartheta + C\sigma}\right)^{\frac{cdqK}{r(1 + bx_1)(1 + bx_2)}}, \tag{18}$$

solution (17) *exhibits the asymptotic stability. where* σ *and* ϑ *are defined in the proof below.*

Proof For $\tau = 0$, let

$$P(x, y) = \frac{r}{1 + ay}x\left(1 - \frac{x}{K}\right) - \nu - \frac{e^{-\varepsilon\nu}qxy}{1 + bx} = -\frac{r}{K(1 + ay)}(x - x_1)(x - x_2) - \frac{e^{-\varepsilon\nu}qxy}{1 + bx},$$

$$Q(x, y) = \frac{ce^{-\varepsilon\nu}qxy}{1 + bx} - my, \qquad \alpha = -\frac{px^2}{x + h}, \qquad \beta = \frac{\tau}{1 + \delta y}, \qquad \phi = x - ET,$$

$$\left(x^T\left(T^+\right), y^T\left(T^+\right)\right) = \left((1 - \theta)ET, 0\right), \qquad \left(x^T(T), y^T(T)\right) = (ET, 0).$$

Since $d = e^{-\varepsilon\nu}$, we can determine the value by performing the calculation

$$\frac{\partial P}{\partial x} = \frac{r}{1+ay} - \frac{2r}{K(1+ay)}x - \frac{dqy}{(1+bx)^2}, \qquad \frac{\partial Q}{\partial y} = \frac{cdqx}{1+bx} - m, \qquad \frac{\partial \phi}{\partial x} = 1,$$
$$\frac{\partial \alpha}{\partial x} = -\frac{px^2+2phx}{(x+h)^2}, \qquad \frac{\partial \beta}{\partial y} = -\frac{\tau\delta}{(1+\delta y)^2}, \qquad \frac{\partial \alpha}{\partial y} = \frac{\partial \beta}{\partial x} = \frac{\partial \phi}{\partial y} = 0.$$

Then

$$\begin{aligned}\Delta_1 &= \frac{P_+(\frac{\partial \beta}{\partial y}\frac{\partial \phi}{\partial x} - \frac{\partial \beta}{\partial x}\frac{\partial \phi}{\partial y} + \frac{\partial \phi}{\partial x}) + Q_+(\frac{\partial \alpha}{\partial x}\frac{\partial \phi}{\partial y} - \frac{\partial \alpha}{\partial y}\frac{\partial \phi}{\partial x} + \frac{\partial \phi}{\partial y})}{P\frac{\partial \phi}{\partial x} + Q\frac{\partial \phi}{\partial y}} \\ &= \frac{P_+(x^T(T^+), y^T(T^+))(1-\tau\delta)}{P(x^T(T), y^T(T))} \\ &= \frac{[(1-\theta)ET - x_1][(1-\theta)ET - x_2](1-\tau\delta)}{(ET-x_1)(ET-x_2)}. \end{aligned} \tag{19}$$

Additionally, let us consider

$$\begin{aligned}&\int_0^T \left[\frac{\partial P}{\partial x}\big(x^T(t), y^T(t)\big) + \frac{\partial Q}{\partial y}\big(x^T(t), y^T(t)\big)\right] dt \\ &= \int_0^T \left[r - m - \frac{2r}{K}x^T(t) + \frac{cdqx^T(t)}{1+bx^T(t)}\right] dt \\ &= (r-m)T - \int_0^T \frac{2r}{K}x^T(t)\,dt + \int_0^T \frac{cdqx^T(t)}{1+bx^T(t)}\,dt, \end{aligned} \tag{20}$$

where

$$\begin{aligned}\int_0^T \frac{2r}{K}x^T(t)\,dt &= \frac{2r}{K}\left(x_1\int_0^T \frac{1}{1+Ce^{\xi t}}\,dt + x_2\int_0^T \frac{Ce^{\xi t}}{1+Ce^{\xi t}}\,dt\right) \\ &= \frac{2r}{K}\left[x_1T - \frac{x_1}{\xi}In\big(1+Ce^{\xi t}\big)\big|_0^T + \frac{x_2}{\xi}In\big(1+Ce^{\xi t}\big)\big|_0^T\right] \\ &= \frac{2rx_1}{K}T + \frac{2r}{K\xi}(x_2-x_1)In\frac{1+Ce^{\xi T}}{1+C}\end{aligned}$$

and

$$\begin{aligned}\int_0^T \frac{cdqx^T(t)}{1+bx^T(t)}\,dt &= \int_0^T \frac{cdq(x_1+x_2Ce^{\xi t})}{1+Ce^{\xi t}+bx_1+bx_2Ce^{\xi t}}\,dt \\ &= \int_0^T \frac{cdqx_1+cdqx_2Ce^{\xi t}}{(1+bx_1)+(1+bx_2)Ce^{\xi t}}\,dt = A_1 + A_2,\end{aligned}$$

where

$$\begin{aligned}A_1 &= cdqx_1\int_0^T \frac{1}{(1+bx_1)+(1+bx_2)Ce^{\xi t}}\,dt \\ &= \frac{cdqx_1}{1+bx_2}\int_0^T \frac{1}{(1+bx_1)/(1+bx_2)+Ce^{\xi t}}\,dt\end{aligned}$$

$$= \frac{cdqx_1}{1+bx_2}\frac{1+bx_2}{1+bx_1}\left(T - \frac{1}{\xi}In\left((1+bx_1)/(1+bx_2) + Ce^{\xi t}\right)\Big|_0^T\right)$$
$$= \frac{cdqx_1}{1+bx_1}\left(T - \frac{1}{\xi}In\frac{(1+bx_1)/(1+bx_2) + Ce^{\xi T}}{(1+bx_1)/(1+bx_2) + C}\right),$$

and

$$A_2 = cdqx_2\int_0^T \frac{Ce^{\xi t}}{(1+bx_1) + (1+bx_2)Ce^{\xi t}}\,dt$$
$$= \frac{cdqx_2}{(1+bx_2)\xi}In\frac{(1+bx_1)/(1+bx_2) + Ce^{\xi t}}{(1+bx_1)/(1+bx_2) + C}.$$

Based on (16), substitute T into the results of the above calculation and define $\vartheta = \frac{1+bx_1}{1+bx_2}$ and $\sigma = \frac{(ET-x_1)[x_2-(1-\theta)ET]}{[(1-\theta)ET-x_1](x_2-ET)}$. Hence (20) is calculated as

$$\begin{aligned}\int_0^T \left(\frac{\partial P}{\partial x} + \frac{\partial Q}{\partial y}\right)dt &= \frac{r-m}{\xi}In\sigma - \frac{2rx_1}{K\xi}In\sigma + 2In\frac{1+C\sigma}{1+C} - \frac{cdqx_1}{(1+bx_1)\xi}In\sigma \\ &\quad + \frac{cdqx_1}{(1+bx_1)\xi}In\frac{\vartheta + C\sigma}{\vartheta + C} + \frac{cdqx_2}{(1+bx_2)\xi}In\frac{\vartheta + C\sigma}{\vartheta + C} \\ &= \frac{1}{\xi}In\sigma\left(r - m - \frac{2rx_1}{K} + \frac{cdqx_1}{1+bx_1}\right) + 2In\frac{1+C\sigma}{1+C} \\ &\quad + \left[\frac{1}{\xi}\left(\frac{cdqx_2}{1+bx_2} - \frac{cdqx_1}{1+bx_1}\right)\right]In\frac{\vartheta + C\sigma}{\vartheta + C}. \end{aligned} \tag{21}$$

According to (15), (19), (21), and ξ (defined in (14)), the Floquet multiplier

$$\begin{aligned} u_2 &= \Delta_1 \exp\left[\int_0^T \left(\frac{\partial P}{\partial x} + \frac{\partial Q}{\partial y}\right)dt\right] \\ &= \Delta_1\sigma^{[1-\frac{1}{x_2-x_1}(\frac{Km}{r} - \frac{cdqKx_1}{r(1+bx_1)})]}\left(\frac{1+C}{1+C\sigma}\right)^2\left(\frac{\vartheta + C\sigma}{\vartheta + C}\right)^{\frac{cdqK}{r(1+bx_1)(1+bx_2)}} \\ &= \frac{[(1-\theta)ET - x_1][(1-\theta)ET - x_2](1-\tau\delta)}{(ET-x_1)(ET-x_2)}\sigma^{[1-\frac{1}{x_2-x_1}(\frac{Km}{r} - \frac{cdqKx_1}{r(1+bx_1)})]} \\ &\quad \times \left(\frac{1+C}{1+C\sigma}\right)^2\left(\frac{\vartheta + C\sigma}{\vartheta + C}\right)^{\frac{cdqK}{r(1+bx_1)(1+bx_2)}} \\ &= \sigma^{-\frac{1}{x_2-x_1}(\frac{Km}{r} - \frac{cdqKx_1}{r(1+bx_1)})}\left(\frac{\vartheta + C\sigma}{\vartheta + C}\right)^{\frac{cdqK}{r(1+bx_1)(1+bx_2)}}. \end{aligned}$$

After obtaining an expression for u_2, we now discuss the conditions under which u_2 is less than 1. Based on the inequality $x_1 < (1-\theta)ET < ET < x_2$, we can conclude that $ET - x_1 > (1-\theta)ET - x_1$ and $x_2 - (1-\theta)ET > x_2 - ET$, so there are $\sigma > 1$ and $\frac{\vartheta + C\sigma}{\vartheta + C} > 1$. Adding $\frac{cdqK}{r(1+bx_1)(1+bx_2)} > 0$ generates $(\frac{\vartheta + C\sigma}{\vartheta + C})^{\frac{cdqK}{r(1+bx_1)(1+bx_2)}} > 1$. Therefore, for any $\theta \in (0,1)$, when condition (18) is satisfied, we obtain that $u_2 < 1$, and the solution $(x^T(t), 0)$ is locally stable. □

Given the above inference, under the premise of $\tau = 0$, when condition $x_1 < x < x^*$ is met, the solution $(x^T(t), 0)$ is locally stable, as illustrated in Fig. 7, it is evident that y_k^+ diminishes with the progression of k, and $\lim_{k\to\infty} y_k^+ = 0$. Therefore the solution $(x^T(t), 0)$ is

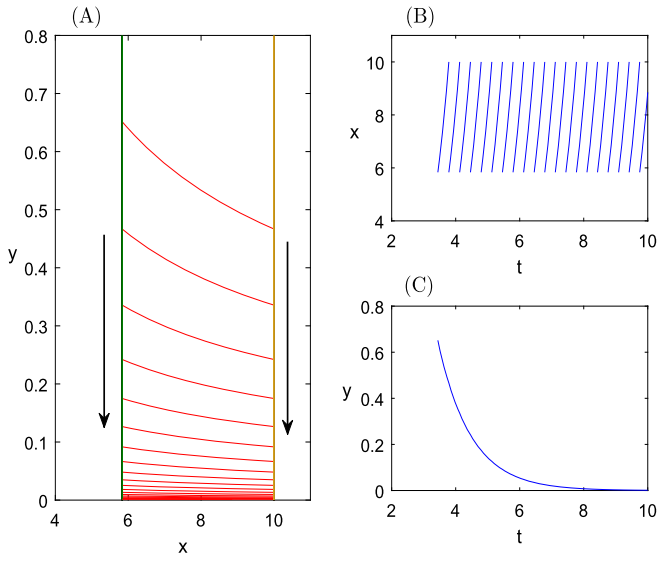

Figure 7 Stability of the solution $(x^T(t), 0)$ with parameters $r = 2$, $K = 50$, $q = 0.2$, $a = 0.005$, $c = 0.5$, $v = 0.4$, $\varepsilon = 0.8$, $m = 1.4$, $b = 0.04$, $p = 0.5$, $h = 2$, $\delta = 1$, $\tau = 0$, $ET = 10$

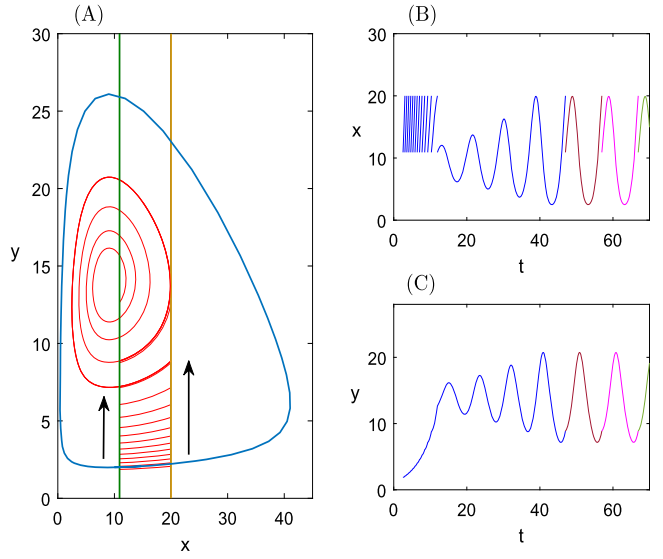

Figure 8 Instability of boundary periodic solution $(x^T(t), 0)$ with parameters $m = 0.484$ and $ET = 20$. The other parameters are consistent with Fig. 7

globally attractive. When condition $x^* < x < x_2$ is met, the solution $(x^T(t), 0)$ is no longer stable, as illustrated in Fig. 8.

Examining subfigures Fig. 7(B) and 7(C), it becomes evident that when the boundary periodic solution stabilizes, x will oscillate periodically with higher frequencies over time t, whereas y will gradually decrease and disappear over time t. From subfigures Fig. 8(B) and 8(C), when the boundary periodic solution is unstable, both x and y will transition from the exterior to the interior of the limit cycle under the influence of pulse control, and

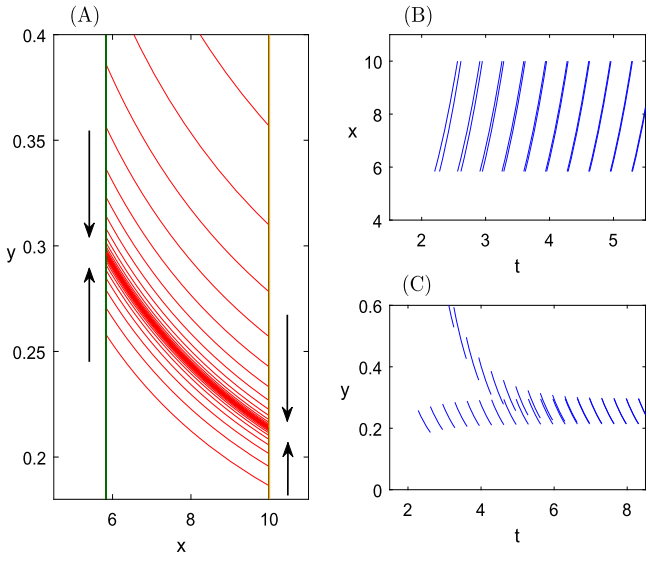

Figure 9 Solution of model (1). Here $\tau = 0.1$. The remaining parameters are consistent with Fig. 7

the transformation process converges toward the limit cycle, ultimately achieving stability in a first-order periodic solution within the confines of the limit cycle.

Based on the above facts, model (1) possesses a stable boundary solution. To more clearly see the impact of pulse control on system (1), we used different values of τ for numerical simulation, as depicted in Fig. 9, and the observation reveals that as the parameter τ varies from 0 to 0.1, system (1) manifests an intrinsic periodic solution regardless of the initial value. In this periodic solution, both x and y coexist over time.

5.2 Order-*k* positive periodic solution with $\tau \neq 0$

In the illustration provided by Fig. 9, it is evident that for any positive value of τ, no matter how small, system (1) exhibits a first-order periodic solution. This implies an increased complexity in the dynamics of the system. Our primary focus of this section is on examining the properties of internal solution when $\tau > 0$, especially the existence and stability of order-1 periodic solution, as well as the existence of order-k periodic solution. This aim can be achieved by demonstrating the presence and stability of the fixed point of the Poincaré map $\varphi(y_k^+)$.

There is a threshold condition for the existence of order-1 periodic solution in case J_{21}.

Theorem 7 *For case J_{21}, there is at least one fixed point for map $\varphi(y_k^+)$.*

Proof From the phase portrait Fig. 5(B) of case J_{21} we can see that the trajectory Γ_1 and L_4 intersect at point $Q_1(ET, y_{Q_1})$, and point Q_1 transitions to point $Q_1^+((1-\theta)ET, y_{Q_1^+})$ after passing through the pulse effect. If $\varphi(y_{Q_0}) = y_{Q_1^+} = y_{Q_0}$, then it is apparent that y_{Q_0} serves as a fixed point for $\varphi(y_k^+)$.

For case J_{21}(a), if $y_{Q_1^+} \neq y_{Q_0}$, whether Q_1^+ is above or below Q_0, the trajectory starting from point Q_1^+ will intersect with L_4 below point Q_1, with a point of intersection of Q_2. After the pulse effect, the pulse point of Q_2 is marked as $Q_2^+((1-\theta)ET, y_{Q_2^+})$. Since the pulse function

$f(y)$ is increasing on the interval $[0, y_{Q_1}]$, when $y_{Q_2} < y_{Q_1}$, there is $y_{Q_2^+} < y_{Q_1^+}$, which is

$$\varphi(y_{Q_1^+}) < y_{Q_1^+}. \tag{22}$$

On the flip side, $f(0) = \tau$ signifies the lowest value of $f(y)$. Hence there is a lowest pulse point in the L_3, denoted as $Q_\tau^+((1-\theta)ET, \tau)$, such that

$$\varphi(\tau) > \tau. \tag{23}$$

From (22) and (23), by the continuity of $\varphi(y_k^+)$ the latter has at least one fixed point on $(\tau, y_{Q_1^+})$.

For case J_{21}(b), if $y_{Q_1^+} \neq y_{Q_0}$, then since the pulse function $f(y)$ is decreasing on the interval $[0, y_{Q_1}]$, we have

$$\varphi(y_{Q_1^+}) > y_{Q_1^+}. \tag{24}$$

On the flip side, $f(0) = \tau$ signifies the highest value of $f(y)$, and Q_τ^+ is the highest pulse point, which yields

$$\varphi(\tau) < \tau. \tag{25}$$

From (24) and (25), by the continuity of $\varphi(y_k^+)$ the latter has at least one fixed point on $(y_{Q_1^+}, \tau)$.

For case J_{21}(c), if $y_{Q_1^+} > y_{Q_0}$, then the inequality $\varphi(y_{Q_0}) > y_{Q_0}$ is established. According to the previous description of the set $\mathcal{N}$, the maximum value of the pulse function $f(y)$ is y_τ^1, and the highest defined pulse point is $Q_{\tau 1}^+((1-\theta)ET, y_\tau^1)$, and thus we have $\varphi(y_\tau^1) < y_\tau^1$. Therefore $\varphi(y_k^+)$ has a fixed point on (y_{Q_0}, y_τ^1). Similarly, if $y_{Q_1^+} < y_{Q_0}$, then $\varphi(y_{Q_0}) < y_{Q_0}$, and the lowest pulse point is Q_δ^+ (defined in Remark 4), and thus $\varphi(y_{Q_\delta^+}) > y_{Q_\delta^+}$. Therefore the map $\varphi(y_k^+)$ possesses a fixed point on $(y_{Q_\delta^+}, y_{Q_0})$. □

Since in case J_{22}, where $y_k^+ \in (y_{P_2}, y_{P_1})$, the solution trajectory starting from L_3 will not reach the pulse set, based on this premise, we obtain the following theorem.

Theorem 8 *For case J_{22}, if $y_{T^+} \geq y_{P_1}$ or $y_{T^+} \leq y_{P_2}$, then the mapping $\varphi(y_k^+)$ possesses at least a single fixed point.*

Proof According to the description of the solution trajectory in phase portrait Fig. 5(C), for case J_{22}, curve Γ_2 intersects line L_4 at point $T(ET, y_T)$ with a tangent relationship. If $y_{T^+} = y_{P_1}$ or $y_{T^+} = y_{P_2}$, then in that way, $\varphi(y_k^+)$ must have a fixed point.

For case J_{22}(a), if $y_{T^+} > y_{P_1}$, then $\varphi(y_{P_1}) > y_{P_1}$. In addition, the solution trajectory starting from point T^+ and line L_4 will intersect at point T_1 below point T satisfying $y_{T_1} < y_T$. Since the pulse function $f(y)$ is increasing under this condition, there is $y_{T_1^+} < y_{T^+}$ such that

$$\varphi(y_{T^+}) < y_{T^+}. \tag{26}$$

Therefore the mapping $\varphi(y_k^+)$ possesses a single fixed point on (y_{P_1}, y_{T^+}).

On the other hand, if $y_{T^+} < y_{P_2}$, then $\varphi(y_{P_2}) < y_{P_2}$. In addition, there is a point $R^+((1-\theta)ET, y_{R^+})$ below point T^+ that satisfies $y_{R^+}(1+\delta y_{R^+}) < \tau$. The trajectory starting from point R^+ intersects with L_4 at point R_1 such that $y_{R_1} < y_{R^+}$. Therefore

$$y_{R^+} < \frac{\tau}{1+\delta y_{R_1}} = y_{R_1^+} = \varphi(y_{R^+}), \tag{27}$$

where R_1^+ is the pulse point of R_1. Then $\varphi(y_k^+)$ has a fixed point on (y_{R^+}, y_{P_2}).

For case J_{22}(b), if $y_{T^+} > y_{P_1}$, then $\varphi(y_{P_1}) > y_{P_1}$. Additionally, according to the previous definition of the phase set, in this case, $f(0) = \tau$ is the maximum value of the ordinate of pulse point in the phase set, which yields $\varphi(\tau) < \tau$. Therefore the map $\varphi(y_k^+)$ has at least one fixed point on (y_{P_1}, τ).

On the other hand, if $y_{T^+} < y_{P_2}$, then $\varphi(y_{P_2}) < y_{P_2}$. Additionally, T_1 is located below point T, and since $f(y)$ is decreasing, $y_{T_1^+} = \varphi(y_{T^+}) > y_{T^+}$. Therefore the map $\varphi(y_k^+)$ has at least one fixed point on $(y_{T_1^+}, y_{P_2})$.

For case J_{22}(c), if $y_{T^+} > y_{P_1}$, then $\varphi(y_{P_1}) > y_{P_1}$. Moreover, $f(y)$ first decreases and then increases on $[0, y_T]$ with a maximum value of y_τ^2. We can define the highest pulse point on the phase set as $P_{\tau 2}^+((1-\theta)ET, y_{P_{\tau 2}^+})$, which easily yields $\varphi(y_{P_{\tau 2}^+}) < y_{P_{\tau 2}^+}$. This indicates the existence of a fixed point of $\varphi(y_k^+)$ on the interval $(y_{P_1}, y_{P_{\tau 2}^+})$.

On the other hand, if $y_{T^+} < y_{P_2}$, then $\varphi(y_{P_2}) < y_{P_2}$. Moreover, the lowest pulse point on the phase set is Q_δ^+, which yields $\varphi(y_{Q_\delta^+}) > y_{Q_\delta^+}$. This indicates the existence of a fixed point of $\varphi(y_k^+)$ on the interval $(y_{Q_\delta^+}, y_{P_2})$. □

To further verify the above conclusions, numerical simulations were conducted for case J_{22}(a), as shown in Fig. 10. It is not difficult to see from Fig. 10(A) that the solution trajectory starting from point P_1, under the action of two pulse effects, reaches T^+ and T_1^+ successively, resulting in two pulse segments, and the larger the y_k, the greater the slope ζ_k, which also reflects the third property in Theorem 5.

Theorems 7 and 8 imply that $\varphi(y_k^+)$ consistently possesses a value of y for which $\varphi(y) = 0$. Afterward, assuming that the fixed point of $\varphi(y_k^+)$ is $\bar{y}$, it is unique. According to the properties of the solution and the above reasoning, we know that $\varphi(y_k^+) < y_k^+$ when $y_k^+ > \bar{y}$ and $\varphi(y_k^+) > y_k^+$ when $y_k^+ < \bar{y}$.

Now let us delve into the stability analysis of $\bar{y}$. This can be established by demonstrating the convergence of the following limit:

$$\lim_{i \to +\infty} \varphi^i(y_k^+) = \bar{y}, \tag{28}$$

where $y_k^+ \in [0, +\infty)$, and $i \geq 1$ are positive integers.

Theorem 9 *For cases $J_{21}(a)$, if either $\varphi(y_{Q_0}) < y_{Q_0}$ or $\varphi(y_{Q_0}) > y_{Q_0}$ with $\varphi^2(y_k^+) > y_k^+$ for $y_k^+ \in [y_{Q_0}, \bar{y})$, then $\bar{y}$ is globally stable. For case $J_{21}(b)$, if either $\varphi(y_{Q_0}) > y_{Q_0}$ or $\varphi(y_{Q_0}) < y_{Q_0}$ with $\varphi^2(y_k^+) < y_k^+$ for $y_k^+ \in (\bar{y}, y_{Q_0}]$, then $\bar{y}$ is globally stable.*

Proof By Theorem 7 a fixed point for $\bar{y}$ exists in the case of J_{21}.

In case J_{21}(a), when $\varphi(y_{Q_0}) < y_{Q_0}$, obviously, $\bar{y} < y_{Q_0}$. We will address three intervals separately. (1) If $y_k^+ \in [0, \bar{y})$, then $y_k^+ < \varphi(y_k^+) < \bar{y}$, and since $\varphi(y_k^+)$ is increasing in this case, $\varphi(y_k^+) < \varphi^2(y_k^+) < \bar{y}$, and so on, $\varphi^{i-1}(y_k^+) < \varphi^i(y_k^+) < \bar{y}$. Additionally, treating $\varphi^i(y_k^+)$ as

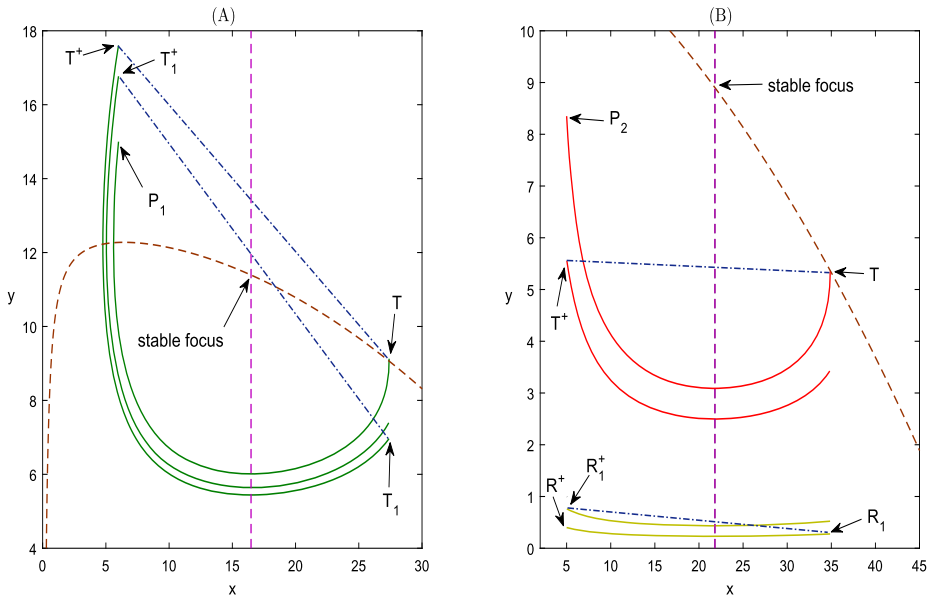

Figure 10 The solution curve associated with model (1) in case J_{22}(a). (A) $y_{T^+} > y_{P_1}$; (B) $y_{T^+} < y_{P_2}$

a function of i yields limit (28). (2) If $y_k^+ \in (\bar{y}, y_{Q_0}]$, then $\bar{y} < \varphi(y_k^+) < y_k^+$. Like in case (1), $\bar{y} < \varphi^i(y_k^+) < \varphi^{i-1}(y_k^+)$. Hence limit (28) is established. (3) If $y_k^+ \in (y_{Q_0}, +\infty)$, then according to the properties of the solution, there must be $\varphi(y_k^+) \in (0, y_{Q_0})$, indicating that

$$\lim_{i \to +\infty} \varphi^{i+1}\left(y_k^+\right) = \bar{y}.$$

Therefore, when $\varphi(y_{Q_0}) < y_{Q_0}$, $\bar{y}$ is globally stable.

On the other hand, when $\varphi(y_{Q_0}) > y_{Q_0}$ and, obviously, $\bar{y} > y_{Q_0}$, we also consider two intervals. (1) If $y_k^+ \in [y_{Q_0}, \bar{y})$, then $\varphi(y_k^+)$ is decreasing, which means that $\bar{y} < \varphi(y_k^+) < \varphi(y_{Q_0})$. In addition, the relationship $\varphi^2(y_k^+) > y_k^+$ yields $y_k^+ < \varphi^2(y_k^+) < \bar{y}$. Further, we obtain $\bar{y} < \varphi^3(y_k^+) < \varphi(y_k^+)$, $\varphi^2(y_k^+) < \varphi^4(y_k^+) < \bar{y}$, and so on, $\varphi^{2i-2}(y_k^+) < \varphi^{2i}(y_k^+) < \bar{y}$. Therefore, limit (28) is established. For intervals (2) $y_k^+ \in [0, y_{Q_0}) \cup (\bar{y}, +\infty)$, we can conclude that there exists a positive integer j_1 such that $\varphi^{j_1}(y_k^+) \in [y_{Q_0}, \bar{y})$. Thereby

$$\lim_{i \to +\infty} \varphi^{2i+j_1}\left(y_k^+\right) = \bar{y}.$$

Therefore, when $\varphi(y_{Q_0}) > y_{Q_0}$ with $\varphi^2(y_k^+) > y_k^+$ for $y_k^+ \in [y_{Q_0}, \bar{y})$, $\bar{y}$ is globally stable.

In the case of J_{21}(b), the proof is analogous to that of case J_{21}(a). □

Theorem 10 *For cases $J_{21}(c)$, if either $\varphi(y_{Q_0}) < y_{Q_0}$, $\varphi(y_d) > y_d$ or $\varphi(y_{Q_0}) > y_{Q_0}$, $\varphi(y_u) < y_u$ with $\varphi^2(y_k^+) < y_k^+$ for $y_k^+ \in (\bar{y}, y_u]$, then the fixed point $\bar{y}$ is globally stable.*

Proof In the case of $\varphi(y_{Q_0}) < y_{Q_0}$, $\varphi(y_d) > y_d$, the fixed point exists in the interval (y_d, y_{Q_0}), we also consider three intervals: (1) $[y_d, \bar{y})$; (2) $(\bar{y}, y_{Q_0}]$; and (3) $(0, y_d) \cup (y_{Q_0}, +\infty)$. For interval (1), we have $y_d \le y_k^+ < \bar{y}$, and since $\varphi(y_k^+)$ is increasing, it follows that $y_k^+ < \varphi(y_k^+) < \bar{y}$. After repeated multiple times, resulting in $\varphi^{i-1}(y_k^+) < \varphi^i(y_k^+) < \bar{y}$, we can note that with the increasing value of i, $\varphi^i(y_k^+)$ likewise increases and gradually converges toward $\bar{y}$.

Thus limit (28) is established. For interval (2), we have $\bar{y} < y_k^+ \le y_{Q_0}$, so we can also get $\bar{y} < \varphi^i(y_k^+) < \varphi^{i-1}(y_k^+)$. Thus limit (28) is established. For interval (3), there is a number j_2 such that $\varphi^{j_2}(y_k^+) \in [y_a, y_{Q_0}]$ leads to

$$\lim_{i\to+\infty} \varphi^{i+j_2}\left(y_k^+\right) = \bar{y},$$

and thus $\bar{y}$ is globally stable.

On the other hand, in the case of $\varphi(y_{Q_0}) > y_{Q_0}$, $\varphi(y_u) < y_u$, the fixed point is in the interval (y_{Q_0}, y_u), and we consider the following two intervals: (1) $(\bar{y}, y_u]$ and (2) $(0, \bar{y}) \cup (y_u, +\infty)$. For interval (1), since $\varphi(y_k^+)$ is decreasing, we have $\bar{y} < \varphi^2(y_k^+) < y_k^+$, from which it follows that $\bar{y} < \varphi^4(y_k^+) < \varphi^2(y_k^+)$, and for all $i \ge 1$, we have $\bar{y} < \varphi^{2i}(y_k^+) < \varphi^{2i-2}(y_k^+)$, which means that limit (28) is established. For interval (2), there exists a positive integer j_3 such that $\varphi^{j_3}(y_k^+) \in (\bar{y}, y_u]$, which leads to

$$\lim_{i\to+\infty} \varphi^{2i+j_3}\left(y_k^+\right) = \bar{y}.$$

Therefore $\bar{y}$ is globally stable. □

Theorem 11 *For case $J_{22}(d)$, if $\varphi(y_{P_2}) < y_{P_2}$ or, alternatively, if $\varphi(y_{P_1}) > y_{P_1}$ has $\varphi^2(y_k^+) > y_k^+$ for all $y_k^+ \in [y_{P_1}, \bar{y})$ and satisfies $\tau \ge y_{P_1}$, then $\bar{y}$ is globally stable. For case $J_{22}(e)$, if $\varphi(y_{P_1}) > y_{P_1}$ or, alternatively, if $\varphi(y_{P_2}) < y_{P_2}$ has $\varphi^2(y_k^+) < y_k^+$ for all $y_k^+ \in (\bar{y}, y_{P_2}]$ and satisfies $\tau \le y_{P_2}$, then $\bar{y}$ is globally stable.*

Proof By Theorem 8, for case J_{22}, if $y_{T^+} \ge y_{P_1}$ or $y_{T^+} \le y_{P_2}$, then $\varphi(y_k^+)$ has a fixed point.

For case J_{22}(d), if $\varphi(y_{P_2}) < y_{P_2}$, then the fixed point $\bar{y}$ is below y_{P_2}. Consider intervals (1) $[0, \bar{y})$, (2) $(\bar{y}, y_{P_2}]$, and (3) $[y_{P_1}, +\infty)$, which is consistent with the case J_{21}(a) and $\varphi(y_{Q_0}) < y_{Q_0}$ in Theorem 9.

On the other hand, if $\varphi(y_{P_1}) > y_{P_1}$, then $\bar{y} > y_{P_1}$. Consider two intervals (1) $[y_{P_1}, \bar{y})$ and (2) $[0, y_{P_2}] \cup (\bar{y}, +\infty)$. Because $\varphi(y_k^+)$ is decreasing in the first interval, it is not difficult to see that $\bar{y} < \varphi(y_k^+) \le \varphi(y_{P_1})$. Combining with the given condition $\varphi^2(y_k^+) > y_k^+$, we obtain $y_k^+ < \varphi^2(y_k^+) < \bar{y}$. Similarly, we can infer that $\varphi^{2i-2}(y_k^+) < \varphi^{2i}(y_k^+) < \bar{y}$, so limit (28) is established. For the second interval, since $\varphi(0) = \tau \ge y_{P_1}$, there is a positive integer j_4 such that $\varphi^{j_4}(y_k^+) \in [y_{P_1}, \bar{y})$. Therefore

$$\lim_{i\to+\infty} \varphi^{2i+j_4}\left(y_k^+\right) = \bar{y},$$

and thus $\bar{y}$ is globally stable.

In the case of J_{22}(e), the proof follows a parallel process to that of J_{22}(d). □

Theorem 12 *For cases $J_{22}(f)$, if $\varphi(y_{P_2}) < y_{P_2}$, $\varphi(y_D) > y_D$ or, alternatively, if $\varphi(y_{P_1}) > y_{P_1}$, $\varphi(y_U) < y_U$ with $\varphi^2(y_k^+) > y_k^+$ for $y_k^+ \in [y_{P_1}, \bar{y})$, then $\bar{y}$ is globally stable.*

Proof If $\varphi(y_{P_2}) < y_{P_2}$, $\varphi(y_D) > y_D$, then there is a fixed point $\bar{y}$ in the interval (y_D, y_{P_2}). We consider three intervals: (1) $(\bar{y}, y_{P_2}]$, (2) $[y_D, \bar{y})$, and (3) $[0, y_D) \cup [y_{P_1}, +\infty)$. For the first interval, we have the inequality $\bar{y} < \varphi(y_k^+) < y_k^+$, and $\varphi(y_k^+)$ is increasing, indicating that $\varphi^i(y_k^+)$ decreases with the increase of i and gradually approaches $\bar{y}$. Similarly, for the second interval, $\varphi^i(y_k^+)$ increases with the increase of i and gradually approaches $\bar{y}$, thus obtaining

limit (28). For the third interval, there is a positive integer j_5 such that $\varphi^{j_5}(y_k^+) \in [y_D, y_{P_2}]$. Hence

$$\lim_{i\to+\infty} \varphi^{i+j_5}\left(y_k^+\right) = \bar{y}.$$

On the flip side, if $\varphi(y_{P_1}) > y_{P_1}$, $\varphi(y_U) < y_U$, then $\bar{y}$ is in the interval (y_{P_1}, y_U). We consider two intervals (1) $[y_{P_1}, \bar{y})$ and (2) $[0, y_{P_2}] \cup (\bar{y}, +\infty)$. When $y_{P_1} \le y_k^+ < \bar{y}$, since $\varphi(y_k^+)$ decreasing on the interval $[y_{P_1}, y_U]$, we have $\bar{y} < \varphi(y_k^+) \le \varphi(y_{P_1})$, which, combined with the inequality $\varphi^2(y_k^+) > y_k^+$, yields $y_k^+ < \varphi^2(y_k^+) < \bar{y}$. Thus we can infer that $\varphi^{2i-2}(y_k^+) < \varphi^{2i}(y_k^+) < \bar{y}$, which indicates that limit (28) is established. When y_k^+ belongs to the second interval, there exists a number j_6 such that $\varphi^{j_6}(y_k^+) \in [y_{P_1}, \bar{y})$. Hence

$$\lim_{i\to+\infty} \varphi^{2i+j_6}\left(y_k^+\right) = \bar{y},$$

and thus $\bar{y}$ is globally stable. □

Theorems 9–12 delineate the pertinent conditions for the global stability of the fixed point of $\varphi(y_k^+)$, signifying the global stability of the first-order periodic solution of system (1). We now discuss the order-k ($k \ge 2$) periodic solution and only analyze only cases J_{21}(a) and (b).

According to Theorem 7, we know that system (1) must have an order-1 periodic solution in case J_{21}. Denote it by $(\xi(t), \eta(t))$ and assume that it passes through points $G^+((1-\theta)ET, \eta_0^+)$ and $G(ET, \eta_0)$. Now we give threshold conditions for the existence of only order-1 periodic solution.

Theorem 13 *For cases $J_{21}(a)$, if $y_{Q_1^+} \le y_{Q_0}$, then system (1) exclusively displays an order-1 periodic solution and does not possess an order-2 periodic solution.*

Proof If $y_{Q_1^+} = y_{Q_0}$, then the conclusion is valid. If $y_{Q_1^+} < y_{Q_0}$, then assuming that the initial point of system (1) is Q_1^+, the solution trajectory will reach point Q_2 on the pulse set as the solution trajectories cannot intersect. Therefore Q_2 is below Q_1 and then mapped to Q_2^+ through the pulse effect. Based on the increasing pulse function $f(y)$ in this case, there is Q_2^+ below Q_1^+, which means that y_k^+ decreases as y_k decreases, resulting in that point Q_{k+1}^+ is below point Q_k^+. Hence the sequence $y_{Q_k^+}$ $(k = 1, 2, \ldots, n)$ is decreasing, that is,

$$y_{Q_1^+} > y_{Q_2^+} > y_{Q_3^+} > \cdots > y_{Q_k^+} \cdots > y_{Q_n^+} > \eta_0^+ > 0. \tag{29}$$

It is not difficult to see from relationship (29) that system (1) only exhibits an order-1 without an order-2 periodic solution. □

Similarly, for case J_{21}(b), if $y_{Q_1^+} \ge y_{Q_0}$, then we can arrive at the same conclusion.

Now we give threshold conditions for the existence of order-1 or order-2 periodic solution.

Theorem 14 *For cases $J_{21}(a)$, if $y_{Q_1^+} > y_{Q_0}$ and $y_{Q_2^+} \ge y_{Q_0}$, then system (1) only exhibits order-1 or order-2 without order-3 periodic solution.*

Proof If $y_{Q_1^+} > y_{Q_0}$, $y_{Q_2^+} = y_{Q_0}$, then the conclusion is valid. If $y_{Q_2^+} > y_{Q_0}$, then since $\varphi(y_k^+)$ is decreasing on the interval $[y_{Q_0}, +\infty)$, so $y_{Q_2^+} < y_{Q_1^+}$, the pulse point Q_3^+ corresponding to the solution starting from Q_2^+ will fall into the interval $(y_{Q_2^+}, y_{Q_1^+})$, and then pulse point Q_4^+ corresponding to the solution starting from Q_3^+ will fall into the interval $(y_{Q_2^+}, y_{Q_3^+})$. Therefore $y_{Q_1^+} > y_{Q_3^+} > y_{Q_4^+} > y_{Q_2^+} > y_{Q_0}$. Without loss of generality, after k times of pulse effect, the sequence $y_{Q_k^+}$ satisfies

$$y_{Q_1^+} > y_{Q_3^+} > \cdots > y_{Q_{2n-1}^+} > y_{Q_{2n+1}^+} > \cdots > y_{Q_{2n}^+} > y_{Q_{2n-2}^+} > \cdots > y_{Q_2^+} > y_{Q_0}. \tag{30}$$

According to equation (30), if

$$\lim_{n\to\infty} y_{Q_{2n}^+} = \lim_{n\to\infty} y_{Q_{2n+1}^+} = \eta_0^+, \quad \eta_0^+ \in (y_{Q_2^+}, y_{Q_3^+}),$$

then $\varphi(y_k^+)$ possesses a fixed point. Furthermore, if

$$\lim_{n\to\infty} y_{Q_{2n}^+} = \eta_1^+ \neq \eta_2^+ = \lim_{n\to\infty} y_{Q_{2n+1}^+}, \quad \eta_1^+, \eta_2^+ \in (y_{Q_2^+}, y_{Q_3^+}),$$

then $\varphi(y_k^+)$ has a periodic two-point cycle. Based on the above description, system (1) does not exhibit an order-3 periodic solution. □

Similarly, for case J_{21}(b), if $y_{Q_1^+} < y_{Q_0}$ and $y_{Q_2^+} \leq y_{Q_0}$, then we can arrive at the same conclusion.

Now we proceed to discussing the conditions for the existence of an order-3 periodic solution.

Theorem 15 *For case $J_{21}(a)$, assuming that $y_q^+ = \min\{y_k^+ | \varphi(y_k^+) = y_{Q_0}.\}$, if $\varphi(y_{Q_0}) > y_{Q_0}$ and $\varphi^2(y_{Q_0}) < y_q^+$, then system (1) exhibits an order-3 periodic solution.*

Proof According to the assumed conditions, it is evident that $\varphi(y_k^+)$ possesses a fixed point on $(y_{Q_0}, y_{Q_1^+})$. Therefore we only need to prove that there exists a number $y \in Y_1$ such that $\varphi(y) \neq y$ and $\varphi^3(y) = y$. Indeed, it is easy to obtain

$$\varphi^3(y_q^+) = \varphi^2(y_{Q_0}) < y_q^+, \qquad \varphi^3(0) = \varphi^2(\tau) > 0.$$

By the continuity of $\varphi(y_k^+)$ there exists a number $\tilde{y} \in (0, y_q^+)$ such that $\tilde{y} < y_{Q_0}$ and $\varphi^3(\tilde{y}) = \tilde{y}$. In other words, system (1) has an order-3 periodic solution. □

Theorem 15 indicates that a discrete mapping $\varphi(y_k^+)$ has a periodic point with a minimum period of 3. According to the Sarkovskii theorem, the mapping $\varphi(y_k^+)$ also has periodic points with a minimum period of any positive integer, implying the manifestation of chaotic phenomena in system (1). Consequently, system (1) also possesses order-k periodic solutions with $k > 3$.

5.3 Numerical simulation

When $\tau \neq 0$, conclusions have been derived from Theorems 7–15. Now we employ numerical simulations to validate these theorems. The typical approach is to examine its bifurcation diagram, revealing the system dynamic changes concerning an invariant parameter.

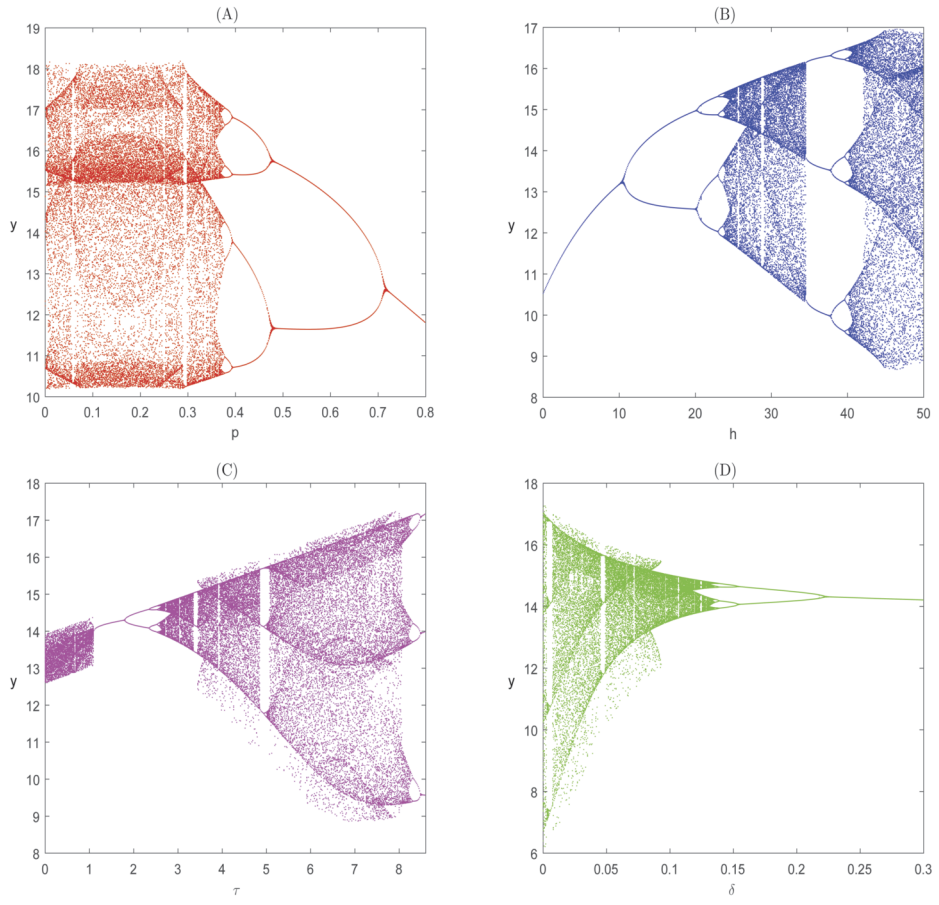

Figure 11 Bifurcation diagram of system (1): (A) with respect to p and $h = 1.6$, $\tau = 10$, $\delta = 0.1$; (B) with respect to h and $p = 0.76$, $\tau = 7.1$, $\delta = 0.1$; (C) with respect to τ and $p = 0.08$, $h = 7.8$, $\delta = 0.1$; (D) with respect to δ and $p = 0.078$, $h = 9$, $\tau = 3.5$. The other parameters are $r = 1$, $K = 50$, $q = 0.2533$, $a = 0.005$, $c = 0.45$, $v = 0.07$, $\varepsilon = 4.11$, $m = 0.36$, $b = 0.19$, $ET = 25$

Consequently, we have depicted the bifurcation diagram of system (1) with respect to p, h, τ, and δ, as illustrated in Fig. 11.

Figure 11(A) shows the bifurcation diagram regarding p. It is easy to see that when $p < 0.3$, the system is in chaos, and in the interval $(0.3, 0.4)$, the system undergoes a transition from a high-order to a low-order periodic solution in the chaotic band, which is the period-halving bifurcation. Afterward, every time the system undergoes such a transition, The order of the periodic solution will undergo halving until $p \approx 0.718$, at which point an order-1 periodic solution will emerge in system (1). This indicates that the system no longer depends on the initial value, and any solution trajectory will tend to the order-1 periodic solution.

Similarly, with h as the bifurcation parameter, the obtained bifurcation diagram can also illustrate the complex dynamics of system (1). From Fig. 11(B) we can see that when $h = 0$ and other parameter values are fixed, the order-1 periodic solution exists, and as h increases within the interval $(0, 30)$, the periodic solution of the system undergoes a rapid transition from order 1 to order 2, and then to order 4, until it enters the chaotic region, indicating the existence of period-doubling bifurcation. When $h \approx 34.5$, the system generates an order-3 periodic solution from the chaotic region, and then h continues to in-

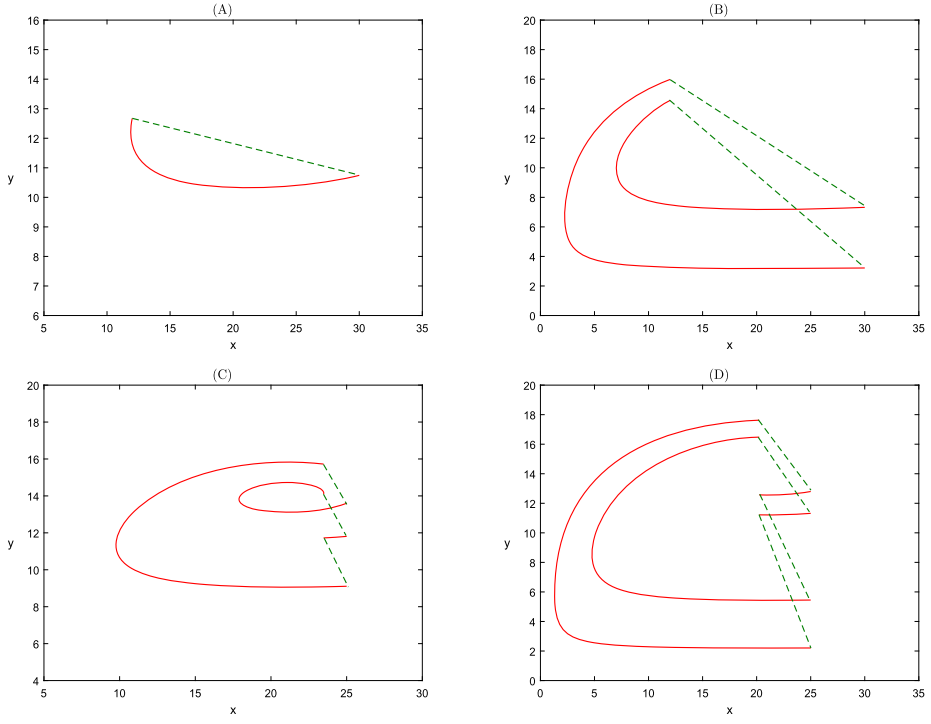

Figure 12 Order-k ($k = 1, 2, 3, 4$) periodic solution of system (1). (A) $p = 0.64$, $h = 2$, $\tau = 4$, $ET = 30$; (B) $p = 0.64$, $h = 2$, $\tau = 15$, $ET = 30$; (C) $p = 0.08$, $h = 7.8$, $\tau = 5$, $ET = 25$; (D) $p = 0.25$, $h = 7.8$, $\tau = 11$, $ET = 25$. The other parameters are consistent with Fig. 11(A)

crease. The period-doubling bifurcation will cause a transition from the order 3 to the order 6 periodic solution until it enters the chaotic region again.

To highlight the impact of nonlinear pulses on the dynamic characteristics of model (1), we then selected τ and δ as bifurcation parameters, as shown in Figs. 11(C) and 11(D). The results demonstrate that the system also displays noteworthy behavior in periodic solution transitions. Figure 11(C) reflects that system (1) has undergone transcritical and period-doubling bifurcations successively, leading to the appearance of order-1 periodic solution and the phenomenon of periodic increases from order k to order $(k + 1)$. Figure 11(D) presents the phenomenon of periodic decreases from order $(k + 1)$ to order k until order 1. These results all indicate that the nonlinear pulse constructed due to resource limitation has a significant impact on the periodic oscillations of two populations; it also shows us the rationality of considering resource limitation in mathematical model related to pest management.

To further understand the impact of resource limitation on the order-k periodic solution. As shown in Fig. 12, we fix all parameter values in the ODE model and only change the parameters related to nonlinear pulse and threshold ET, draw the phase portrait of system (1) from an order-1 to order-4 periodic solution. We can see that within a cycle T (referring to the time interval between x and y passing through the same point), the more complex the trajectory, the greater the pest outbreak period. This indicates that when different pulse strategies are applied, the outbreak mode and frequency of pests change.

Since resource limitation plays a crucial role in comprehensive control measures, the killing rate of pesticides is also a topic that we need to pay special attention to. Based on

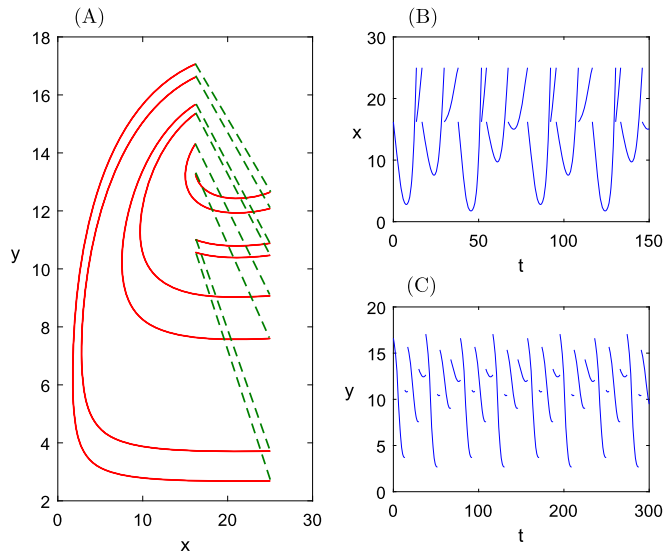

Figure 13 Order-8 periodic solution of system (1) with $p = 0.374$. The other parameters are consistent with Fig. 11(A)

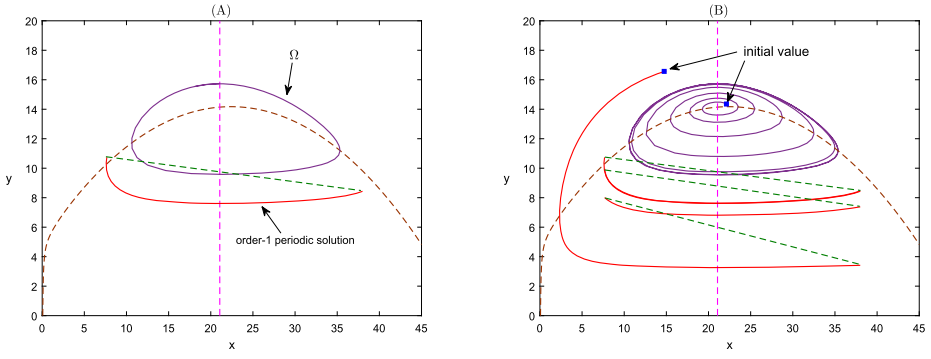

Figure 14 The order-1 periodic solution coexists with limit cycle. The parameters are $p = 0.84$, $h = 2$, $\tau = 14$, $\delta = 0.6$, $ET = 38$, an the other parameters are consistent with Fig. 11

Fig. 11(A), we can see that when $p \approx 0.374$, the chaotic attractor of the system disappears, and a periodic attractor suddenly appears [38]. Therefore we fixed all parameters, taking $p = 0.374$, and the outbreak mode of pests is shown in Fig. 13. The results show that system (1) possesses an order-8 periodic solution, indicating that the pest population will experience eight different degrees of outbreaks within one cycle, and the duration of each outbreak varies, and this can also be seen in the time series in Fig. 13(B). Similar phenomena are also quite common in many nervous systems [39]. In addition, it indicates that the effectiveness of pesticides is also one of the important indicators for pest control strategy.

Of course, in addition to the parameter p, we can see from the bifurcation diagram that changes in parameters h, τ, δ also exacerbate the complexity of system (1). Extensive numerical studies indicate that the system possesses a multistability phenomenon. For example, in Fig. 14 the coexistence of the first-order periodic solution and the limit cycle can be observed, suggesting that the ultimate state of the predator–prey system will be

contingent on the initial values of pests and natural enemies. If the initial value is situated inside the limit cycle, then the system will ultimately converge to the stable limit cycle Ω; if it is outside the limit cycle, then the system will tend to the first-order periodic solution. This result has long been confirmed [12, 40].

6 Conclusions

In the previous pest management models, the effectiveness of insecticides was often considered fixed, thus ignoring the issue of insufficient agricultural resources during pest outbreaks. We established a nonlinear pulse suitable for resource limitation conditions, incorporated the fear effect and the Holling II functional response, and formulated a predator–prey model that accounts for anti-predator behavior. The dynamic behavior of system (1) was mainly studied, and the effects of changes in insecticide fatality rate and natural enemy release on pest outbreaks were expounded.

For the established model, the phase diagram is used to get the range of the phase set and build a Poincaré map. We utilized the properties of the successor function to study the existence and stability of the boundary solution. Figures 7 and 8 mean that under the condition of no artificial release of natural enemies, the number of pests show different periodic oscillations due to different natural enemy mortality and thresholds, but the number of pests will always be controlled within the given threshold range. Furthermore, by the properties of the Poincaré map and nonlinear impulse, the existence conditions for the system to possess order-1 to order-3 periodic solutions are given. In particular, it is expounded that the system can produce periodic solutions of any order in chaos.

The numerical simulation results show that system (1) possesses rich and complex dynamic properties, such as multiple bifurcation types, periodic windows, and chaotic crises. By applying different impulse control strategies pests and natural enemies will eventually coexist in different forms, and pests will also show diversified outbreak patterns. Figures 12 and 13 indicate that the outbreak pattern of pests depends on the selection of sensitive parameters. In addition, we found the coexistence of the order-1 periodic solution and the limit cycle, which reflects that the initial value of system (1) is also an important indicator that affects the global dynamics in a particular case. This helps to provide practical guidance for pest management.

Compared to previous research on impulsive semidynamical systems, the differences in this paper are primarily manifested in the following aspects: (1) Based on the relationship between equilibrium point and threshold, 12 cases are listed, and pulse sets and phase sets are discussed; (2) The existence of parameter h reduces the oscillation amplitude of the solution trajectory of system (1) under resource limitation; (3) The multistability phenomenon of the system makes it possible for pests and natural enemies to coexist in different periodic solutions under the same control strategy; (4) Illustrations of order-1 to order-4 solutions, as well as of order-8 periodic solution, are provided to facilitate a comprehensive understanding of the temporal patterns of pest outbreaks. Nevertheless, it should be noted that the insecticide effect in this paper only targets pests and does not consider the impact on natural enemies or pesticide residues, which can confuse the judgment of optimizing agricultural economic conditions. Therefore adopting appropriate and safe pesticide replacement strategies to improve the economic feasibility of crops will be the focus of our future research.

Acknowledgements
The authors would like to thank the editor and the anonymous reviewers for their constructive comments and suggestions to improve the quality of the paper.

Author contributions
Wenjie Qin: Idea, methodology, project administration, and review editing. Zhengjun Dong: Software, writing, and formal analysis. Both authors read and approved the final manuscript.

Funding
This work is supported by National Natural Science Foundation of China (Nos. 12261104, 12361104) and the Youth Talent Program of Xingdian Talent Support Plan (No. XDYC-QNRC-2022-0708).

Data availability
No data were used for the research described in the paper.

Declarations

Competing interests
The authors declare no competing interests.

Received: 29 January 2024 Accepted: 26 March 2024 Published online: 24 April 2024

References

1. Fitri, I.R., Hanum, F., Kusnanto, A., Bakhtiar, T.: Optimal pest control strategies with cost-effectiveness analysis. Sci. World J. **2021**, 1–17 (2021)
2. Mamta, B., Rajam, M.: RNAi technology: a new platform for crop pest control. Physiology and Molecular Biology of Plants **23**, 487–501 (2017)
3. Raupp, M.J., Holmes, J.J., Sadof, C., Shrewsbury, P., Davidson, J.A.: Effects of cover sprays and residual pesticides on scale insects and natural enemies in urban forests. J. Arboric. **27**(4), 203–214 (2001)
4. Daelemans, R., Hulsmans, E., Laenen, E., Remy, S., Belien, T., Honnay, O.: Direct and indirect effects of management and landscape on biological pest control and crop pest infestation in apple orchards. J. Appl. Ecol. **60**(1), 181–192 (2023)
5. Kungu, M., Deletre, E., Subramanian, S., Fiaboe, K.K., Gitonga, L., Lagat, Z.O., Martin, T.: A new mite IPM strategy: predator avoidance behaviour resulting from the synergetic effects of predator release and acaricide-treated nets. Pest Manag. Sci. **75**(4), 979–985 (2019)
6. Tang, S., Cheke, R.A.: State-dependent impulsive models of integrated pest management (IPM) strategies and their dynamic consequences. J. Math. Biol. **50**, 257–292 (2005)
7. Tian, Y., Tang, S., Cheke, R.A.: Dynamic complexity of a predator–prey model for IPM with nonlinear impulsive control incorporating a regulatory factor for predator releases. Math. Model. Anal. **24**(1), 134–154 (2019)
8. Tang, S., Cheke, R.A.: Models for integrated pest control and their biological implications. Math. Biosci. **215**(1), 115–125 (2008)
9. Tang, S., Liang, J., Tan, Y., Cheke, R.A.: Threshold conditions for integrated pest management models with pesticides that have residual effects. J. Math. Biol. **66**(1–2), 1–35 (2013)
10. Tan, X., Qin, W., Tang, G., Xiang, C., Liu, X., et al.: Models to assess the effects of nonsmooth control and stochastic perturbation on pest control: a pest-natural-enemy ecosystem. Complexity **2019**, 8326164 (2019)
11. Qin, W., Tang, G., Tang, S., et al.: Generalized predator–prey model with nonlinear impulsive control strategy. J. Appl. Math. **2014**, 919242 (2014)
12. Yang, J., Tang, S.: Holling type ii predator–prey model with nonlinear pulse as state-dependent feedback control. J. Comput. Appl. Math. **291**, 225–241 (2016)
13. Baishya, C.: Dynamics of fractional Holling type-II predator–prey model with prey refuge and additional food to predator. J. Appl. Nonlinear Dyn. **10**(02), 315–328 (2021)
14. Tang, S., Tang, G., Cheke, R.A.: Optimum timing for integrated pest management: modelling rates of pesticide application and natural enemy releases. J. Theor. Biol. **264**(2), 623–638 (2010)
15. Zhu, Y., Liu, L., Zhang, Z.: Dynamics of a non-smooth pest-natural enemy model with the threshold control strategy. Phys. Scr. (2023)
16. He, M., Tang, S., Tang, G., Xiang, C.: Bifurcation analysis of an ecological system with state-dependent feedback control and periodic forcing. Int. J. Bifurc. Chaos **31**(15), 2150227 (2021)
17. Tian, Y., Li, H.: The study of a predator–prey model with fear effect based on state-dependent harvesting strategy. Complexity **2022**, 1–19 (2022)
18. Bainov, D.D., Covachev, V.: Impulsive differential equations with a small parameter **24** (1994)
19. Bainov, D.D., Simeonov, P.: Impulsive differential equations: asymptotic properties of the solutions **28** (1995)
20. Bainov, D.D., Simeonov, P.: Impulsive differential equations: periodic solutions and applications (2017)
21. Dubey, B., Kumar, A., et al.: Stability switching and chaos in a multiple delayed prey–predator model with fear effect and anti-predator behavior. Math. Comput. Simul. **188**, 164–192 (2021)
22. Prasad, K.D., Sasmal, S.K.: Dynamics of anti-predator behavior and effect of fear on prey–predator model. J. Biol. Syst. **30**(04), 887–912 (2022)
23. Raw, S., Mishra, P., Tiwari, B.: Mathematical study about a predator–prey model with anti-predator behavior. Int. J. Appl. Comput. Math. **6**, 1–22 (2020)
24. Ives, A.R., Dobson, A.P.: Antipredator behavior and the population dynamics of simple predator–prey systems. Am. Nat. **130**(3), 431–447 (1987)
25. Tang, B., Xiao, Y.: Bifurcation analysis of a predator–prey model with anti-predator behaviour. Chaos Solitons Fractals **70**, 58–68 (2015)

26. Qi, H., Meng, X.: Threshold behavior of a stochastic predator–prey system with prey refuge and fear effect. Appl. Math. Lett. **113**, 106846 (2021)
27. Sarkar, K., Khajanchi, S.: Impact of fear effect on the growth of prey in a predator–prey interaction model. Ecol. Complex. **42**, 100826 (2020)
28. Zhang, H., Cai, Y., Fu, S., Wang, W.: Impact of the fear effect in a prey–predator model incorporating a prey refuge. Appl. Math. Comput. **356**, 328–337 (2019)
29. Wang, X., Zou, X.: Modeling the fear effect in predator–prey interactions with adaptive avoidance of predators. Bull. Math. Biol. **79**, 1325–1359 (2017)
30. Tang, S., Tang, B., Wang, A., Xiao, Y.: Holling II predator–prey impulsive semi-dynamic model with complex Poincaré map. Nonlinear Dyn. **81**, 1575–1596 (2015)
31. Gao, W., Tang, S.: The effects of impulsive releasing methods of natural enemies on pest control and dynamical complexity. Nonlinear Anal. Hybrid Syst. **5**(3), 540–553 (2011)
32. Wilby, A., Thomas, M.B.: Natural enemy diversity and pest control: patterns of pest emergence with agricultural intensification. Ecol. Lett. **5**(3), 353–360 (2002)
33. Wang, X., Tian, Y., Tang, S., et al.: A Holling type II pest and natural enemy model with density dependent IPM strategy. Math. Probl. Eng. **2017**, 8683207 (2017)
34. Qin, W., Tang, S., Cheke, R.A., et al.: The effects of resource limitation on a predator–prey model with control measures as nonlinear pulses. Math. Probl. Eng. **2014**, 450935 (2014)
35. Prasad, K.D., Prasad, B.: Qualitative analysis of additional food provided predator–prey system with anti-predator behaviour in prey. Nonlinear Dyn. **96**(3), 1765–1793 (2019)
36. Hwang, T.-W.: Global analysis of the predator–prey system with Beddington–DeAngelis functional response. J. Math. Anal. Appl. **281**(1), 395–401 (2003)
37. Hwang, T.-W.: Uniqueness of limit cycles of the predator–prey system with Beddington–DeAngelis functional response. J. Math. Anal. Appl. **290**(1), 113–122 (2004)
38. Grebogi, C., Ott, E., Yorke, J.A.: Crises, sudden changes in chaotic attractors, and transient chaos. Phys. D: Nonlinear Phenom. **7**(1–3), 181–200 (1983)
39. Moehlis, J.: Dynamical systems in neuroscience: the geometry of excitability and bursting. SIAM Rev. **50**(2), 397–401 (2008)
40. Jones, W.A., Greenberg, S., Legaspi, B. Jr: The effect of varying Bemisia argentifolii and Eretmocerus mundus ratios on parasitism. BioControl **44**(1), 13–28 (1999)

Publisher's Note